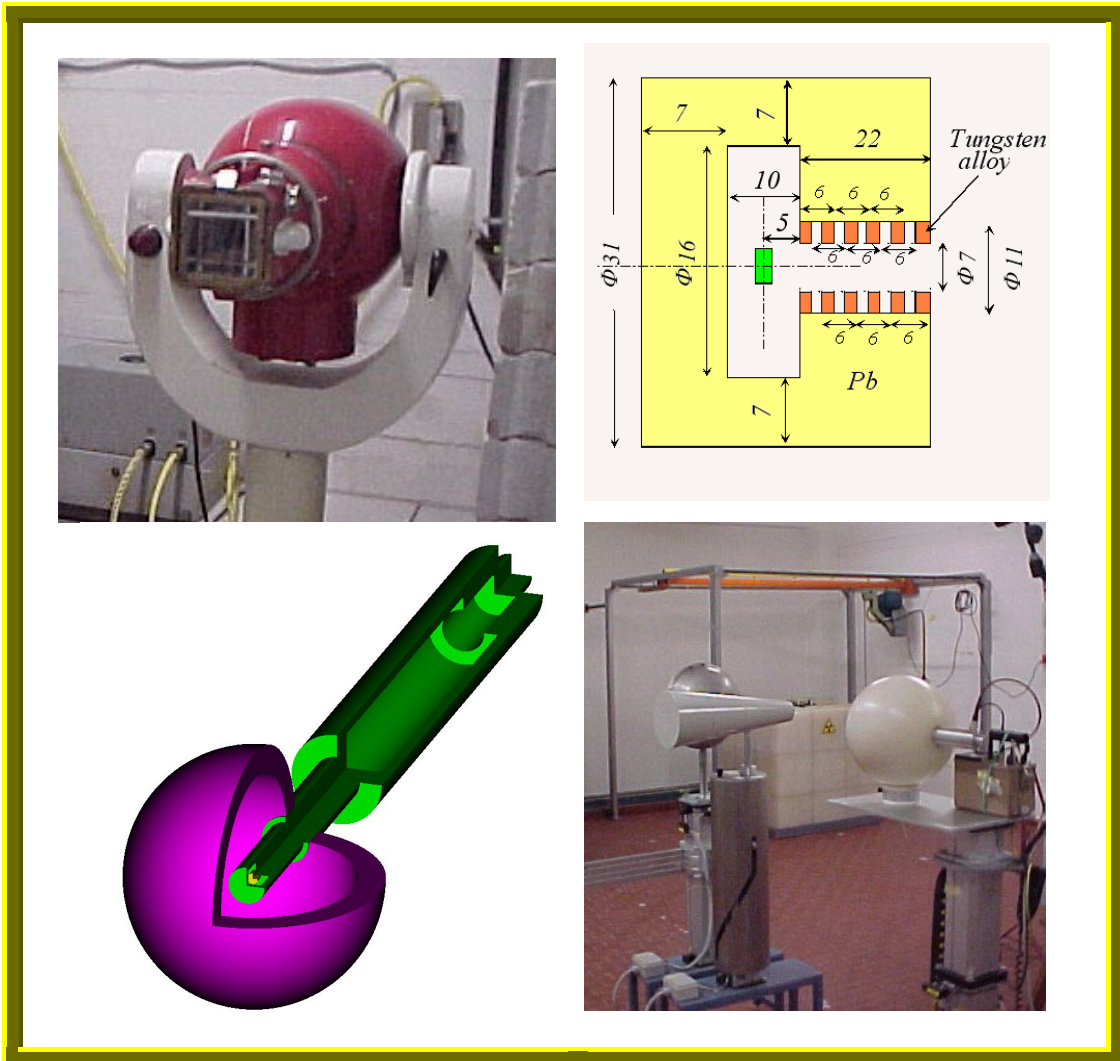


UNCERTAINTY ASSESSMENT IN COMPUTATIONAL DOSIMETRY

An Intercomparison of Approaches



CONRAD
European Union
Coordinated Network for Radiation Dosimetry

Work Package 4
2005 –2007

Updated Version June 2006

FOREWORD

The "Coordination Action" **CONRAD** (*A Coordinated Network for Radiation Dosimetry*) is a project sponsored by the EC within its 6th Framework Programme. Partners of this project are the TU Delft (NL) (administrative coordinator), EURADOS and the University Sankt Gallen (CH).

The CONRAD Project includes four main research coordination Workpackages. Workpackage 4 'Computational Dosimetry' was formed following the tradition of the former EURADOS-Working Group 4 (Numerical Dosimetry) and the EU Concerted Action QUADOS.

This group of specialists in computational dosimetry was in the recent past focused on the quality assurance of the usage of transport calculations in dosimetry. During the 90s a series of Training Courses on Computational Dosimetry were offered and more recently an International Intercomparison on the Usage of Computational Tools for Dosimetry was promoted with a significant participation from various laboratories from Europe and outside.

The project actually combines various research coordination actions in the field of computational dosimetry applied to external and internal exposures at the workplace.

The coordinated activities include intercomparisons and benchmark studies on the overall uncertainty assessment and on the application of advanced tools like voxel models and unfolding techniques for radiation spectra analysis. Special emphasis is given to a close collaboration with the partners undertaking other work packages (WPs) in the project (WP5: Internal Dosimetry, WP6: Complex Radiation Fields and WP7: Medical Staff Dosimetry).

Besides the other goals, CONRAD WP-4 is devoted to encouraging uncertainty assessment in general and in conjunction with computations in particular. Therefore, CONRAD WP-4 starts an action to provide exercises and it distributes a questionnaire in order to find out about the status quo and existing problems. It is hoped to learn from the returns how to better support an increased use of uncertainty assessment in the field of dosimetry for ionizing radiation.

The present proposal, circulated through the EURADOS web site and with direct contact with several laboratories involved in radiation dosimetry is subdivided into three main parts:

- 1- Questionnaire on the status of uncertainty assessment in dosimetry for ionizing radiations. All the contacted laboratories are warmly invited to reply to this very brief questionnaire even if they are not in a condition to take part in the solution in any of the proposed intercomparison problems.
- 2- Intercomparison of computational simulations performed on experimental measurements, for which only the stochastic uncertainties of Monte Carlo solutions should be specified.
- 3- Intercomparison of computational simulations performed on experimental measurements, for which the overall uncertainty budget should be provided or worked out by the participants.

All the participants in the intercomparison are invited to submit their solutions to each problem by December 15th 2006. The replies to the Questionnaire should be returned to to Bernd.Siebert@ptb.de within the same deadline.

Partial solutions are welcome, too.

The submitted results (e.g. detector responses, spectra, etc...) should be presented in ASCII format, that is as simple text (workbook or worksheet format or similar are not welcome).

A final Workshop is planned for the late summer or early autumn 2007, that will be announced soon. The summaries of the anonymous results obtained from the participants will be presented together with some contributions of general relevance to the scope of the WP-4 action. A poster session will be organized for participants who wish to present their solutions explicitly. The Proceedings will appear in 2008.

TO PRESERVE THE SCOPE OF THE COMPARISON ON THE EIGHT PROBLEMS, THE PARTICIPANTS ARE ASKED NOT TO PUBLISH THEIR RESULTS IN THE OPEN LITERATURE BEFORE THE FINAL WORKSHOP (AUTUMN 2007).

CONRAD-WP4
Coordinator
(Gianfranco Gualdrini)

===== CONRAD - Work Package 4 =====

Coordinator: G. Gualdrini

Stefano Agosteo¹, Jean Marc Bordy², Jean-Louis Chartier³, Loic de Carlan⁴, Jose-Maria Gomez Ros⁵, Bernd Großwendt⁶, Gianfranco Gualdrini⁷, Ivan Kodeli⁸, Robert Price⁹, Francesc Salvat¹⁰, Frank Schultz¹¹, Bernd Siebert⁶, Hamid Tagziria¹², Rick Tanner¹³, Michel Terrissol¹⁴, Maria Zankl¹⁵

- 1) Dipartimento di Ingegneria Nucleare, Politecnico di Milano, via Ponzio 34/3, 20133 Milano and INFN, Sezione di Milano, via Celoria 16, 20133 Milano, Italy.
- 2) CEA / DRT – LIST DETECS - LNHB – LMD Bât. 534 91191 Gif sur Yvette CEDEX France
- 3) 18 rue d'Yvette 78690 les Essarts-le-Roi France
- 4) IRSN DRPH SDI LEDI, BP 17, F-92 262, Fontenay-aux-Roses, Cedex, France
- 5) CIEMAT. Av. Complutense 22. E-28040 Madrid, Spain
- 6) PTB, Postfach 3345, D-38023 Braunschweig, Germany
- 7) ENEA ION-IRP, Via dei Colli 16, I-40136 Bologna, Italy
- 8) IAEA representative at OECD-NEA Data Bank Issy Les Moulineaux France
- 9) City University, School of Allied Health Sciences, Northampton Square, London EC1V OHB, UK
- 10) Universitat de Barcelona Facultat de Fisica (ECM) Diagonal 647 08028 Barcelona Spain
- 11) Delft University of Technology, Faculty of Applied Sciences, Mekelweg 15, NL- 2629 JB Delft, The Netherlands
- 12) European Commission Joint Research Centre IPSC TP800 Via Enrico Fermi 21020 Ispra Italy
- 13) HPA, Chilton, Didcot, Oxon OX11 0RG, UK
- 14) CPAT, University Paul Sabatier, 118 route de Narbonne, F-31062 Toulouse Cedex 4, France
- 15) GSF, Ingolstadter Landstrasse 1, D85764 Neuherberg, Germany

Questionnaire on the status of uncertainty assessment in dosimetry for ionizing radiations

Introduction

Generally, the result of a measurement or a computation is only useful and acceptable if a quantitative indication of the quality of the measured or computed value is provided. In science, one uses the *uncertainty* associated with the value and in technical and industrial practice and in health care applications often the so-called expanded uncertainty as a quantitative measure of that quality.

The assessment of uncertainty or expanded uncertainty as a quantitative measure of the quality of a measurement or test result received in recent years increasing attention. One cause for this is the strive for worldwide mutual recognition of measurement or test results in a global economy and the increased awareness for the need of quality assurance, as for instance reflected by the Standard ISO: 17025, issued by the International Standardization Organisation (ISO, Geneva (CH)). Another cause was and still is the publication of the *Guide to the expression of uncertainty in measurement* (GUM: International Organization for Standardization (ISO), Geneva, 1995) that introduced some new concepts and in part a fundamentally different interpretations of uncertainty.

The introduction of the GUM lead to intense and sometimes controversial discussions. However, nowadays, the GUM is increasingly accepted worldwide as the master document for the evaluation of uncertainty. It provides a standard procedure that handles the majority of problems encountered in practice, and – interpreted in terms of Bayesian probability theory– a general procedure that works for the remaining cases. The most important advancement achieved by the GUM is that it accounts for contributions to uncertainty, which arise from the statistics of repeated measurements, termed Type A, and so-called Type B uncertainties. The latter are associated with the values of influencing quantities, which are not measured in a given measurement, but taken from previous measurements, literature, calibration- or testing certificates, product sheets or educated guesses. This is of great importance since Type B contributions generally contribute considerably to the overall uncertainty.

In the field of *dosimetry for ionizing radiation* it is not only necessary to assess uncertainty as a quantitative measure of the quality of a measurement in order to achieve scientific progress but perhaps even more so in applications where in the end human health is at stake. However, in this field one encounters in detail quite some problems in uncertainty assessment. Therefore, one finds in the literature still results without an acceptable statement of uncertainty.

CONRAD Work Package 4 ‘Computational Dosimetry’ (WP4) is devoted to encouraging uncertainty assessment in general and in conjunction with computations in particular. Therefore, WP4 has initiated an action to provide computational exercises and it is distributing a questionnaire in order to establish the status quo and existing problems with the practical realisation of uncertainty assessment and reporting within European laboratories. From the returns, we hope to learn how to better support scientists and better promote an increased use of uncertainty assessment in the field of dosimetry for ionizing radiation.

Correspondence:

The Questionnaire should be returned to:

Bernd Siebert

Bernd.Siebert@ptb.de

within December 15th 2006

Questionnaire on the status of uncertainty assessment in dosimetry for ionizing radiations

In case of multiple choices, please mark the adjacent box.

Part 1: Identification of the participant

We guarantee anonymity, However if you wish to remain anonymous then just fill out P1.4, but indicate the type of facility you work at.

P1.0 Name:

P1.1 Laboratory:

P1.2 Address:

P1.3 EMAIL:

P1.4 Main task:

Part 2: Do you provide any form of calibration service?

P2.0 YES NO

If your answer is NO please turn to **Part 3**.

Within the field of dosimetry for ionizing radiation, the term “calibration” is used for various activities; please briefly characterize your activity:

Your text:

P2.1 *Do you provide this service*

in house to third parties both: in house and to third parties ?

P2.2 *Are you accredited for this service?*

YES NO

If your answer is NO please turn to **Part 3**.

If your answer is YES please provide the name of the accrediting organisation:

Your text:

Part 3: Do you rely on a protocol that requires a function or system to stay within a predefined tolerances?

P3.0 YES NO

If your answer is NO please turn to **Part 4**.

Class 1 Problems

**Expressing only stochastic
Uncertainties**

P1 - RECOIL-PROTON TELESCOPE DETECTOR

Introduction

A monolithic silicon telescope coupled to a polyethylene converter is employed as a recoil-proton spectrometer for neutrons. The telescope consists of a ΔE (1.9 μm thick) stage and an E (500 μm thick) stage realized on a single silicon layer, with active surface $1 \times 1 \text{ mm}^2$. The two stages behave like two adjacent diodes. The dead layer is 0.24 μm thick and composed of titanium. This problem is aimed at calculating the response functions of the two stages to monoenergetic neutrons.

The secondary electrons generated in the structural materials of the detector by the gamma ray background can be discriminated from recoil-protons with coincidence techniques. In this application, the ΔE stage triggers the E stage and only the recoil-protons depositing energy above a threshold in the ΔE stage are accepted. The actual situation is quite complex to simulate and therefore some approximations will be introduced.

Part 1: Problem geometry

The telescope spectrometer can be approximated with a stack of parallelepiped layers. Its cross section (perpendicular to the neutron beam axis) is 1 mm^2 . Consider the irradiation in vacuum.

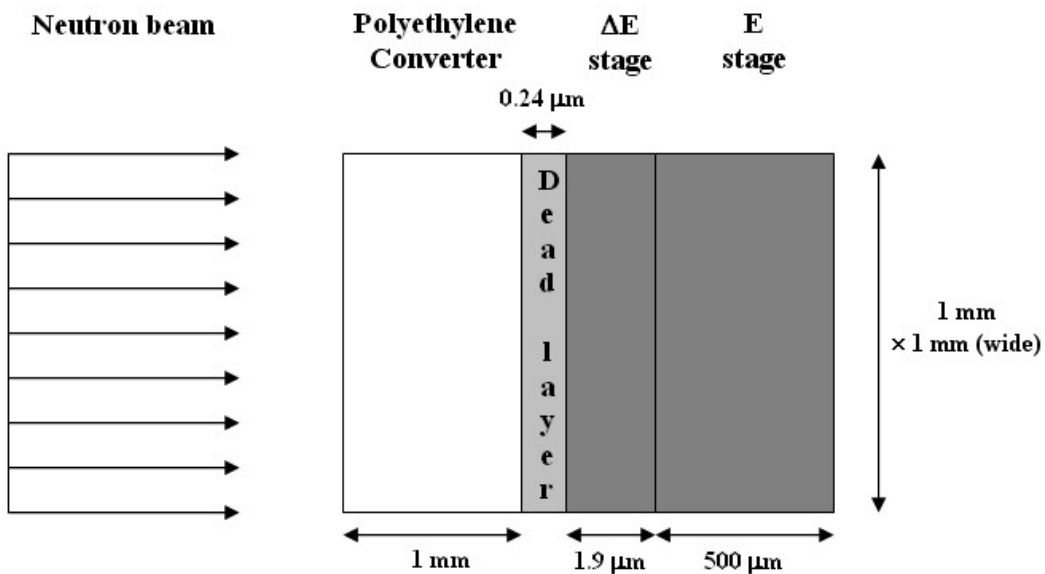


Figure1 : Problem scheme (not to scale) for Part 1

Materials:

Polyethylene (CH_2): density = 0.95 g cm^{-3}

Titanium: density = 4.50 g cm^{-3}

Silicon: density = 2.33 g cm^{-3}

Calculate the response functions (the spectra of energy deposited in silicon, i.e. the “pulse-height” spectrum of recoil-protons) in the ΔE and the E stage when the detector is irradiated by a parallel beam of monoenergetic neutrons. Consider the following neutron energies: 0.680, 0.996 and 1.306 MeV.

Consider parallel beams of neutrons emitted from a rectangular surface ($1 \times 1 \text{ mm}^2$) placed in a vacuum. The results should be normalised to the unit fluence of source neutrons impinging on the detector. A constant energy binning should be set for recording the spectra of energy deposited in silicon. The width of the energy bin should be provided by the participant.

Part 2 (optional)

In order to understand the efficacy of secondary electron discrimination, a very simple approximation is proposed. Treating the actual experimental situation would require the simulation to include the full geometry of the structural parts of the whole detector package (case, connections, cables etc.), the environment in which the irradiation is performed and the spectrum of the gamma rays generated in the target producing monoenergetic neutrons. Therefore, consider the same telescope detector geometry described above and irradiate it with electrons emitted from a rectangular surface ($1 \times 1 \text{ mm}^2$) placed in a vacuum (figure 2). The energy distribution of the source should be uniform in the range 10 keV – 2.5 MeV; the angular distribution of the electron source should be isotropic in the interval from 0 to 90 degrees (polar angle) with respect to the normal to the detector surface (i.e. consider only the electrons emitted in the half-space towards the detector). In this simplified simulation, the rectangular source is placed at 0.1 mm from the dead layer surface and the polyethylene converter should be removed.

Calculate the spectra of energy deposited (i.e., the “pulse-height” spectrum) in the ΔE and the E stage without coincidence and in the E stage triggered by the ΔE stage with a coincidence threshold of 100 keV. The results should be normalised to one source electron. A constant energy binning should be set for the spectra of energy deposited in silicon. The width of the energy bin should be provided by the participant.

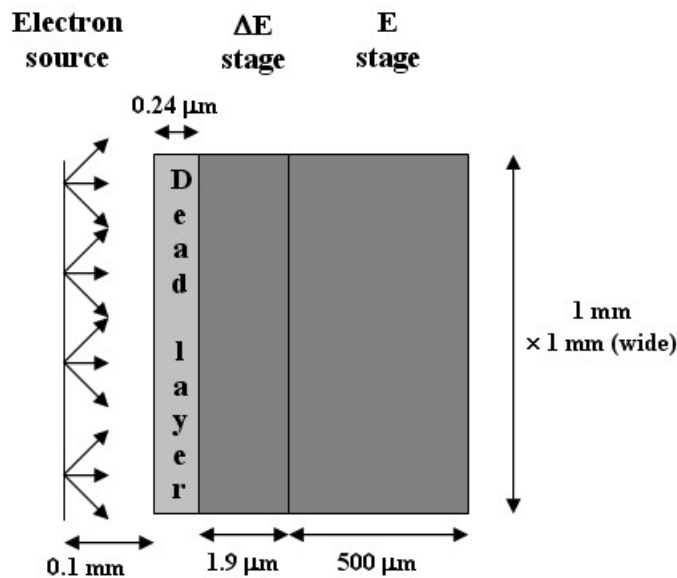


Figure 2: Problem scheme (not to scale) for Part 2

Problem proposed by:

S. Agosteo and A. Pola Dipartimento di Ingegneria Nucleare Politecnico di Milano Italy

TO PRESERVE THE SCOPE OF THE COMPARISON ON THE EIGHT PROBLEMS, THE PARTICIPANTS ARE ASKED NOT TO PUBLISH THEIR RESULTS IN THE OPEN LITERATURE BEFORE THE FINAL WORKSHOP (AUTUMN 2007).

Correspondence:

Results should be returned to:

Stefano Agosteo

Dipartimento di Ingegneria Nucleare

Politecnico di Milano

Via Ponzio 34/3

20133 Milano, Italy - stefano.agosteo@polimi.it

P2 - BONNER SPHERE SPECTROMETER

Introduction

The aim of this problem is to study the response of a widespread neutron spectrometer exposed to the ISO standard neutron sources $^{241}\text{Am-Be}$ and ^{252}Cf .

The instrument is the multi-sphere or Bonner Sphere Spectrometer (BSS), firstly introduced by Bramblett et al [1] in the 60s. The spectrometer is constituted by a set of polyethylene spheres, usually from 6 to 10, with known diameter and density, with an active or passive thermal neutron sensor located at their centre. Since each sphere preferably moderates the neutrons in a given energy range, the set of the measurements obtained from the different spheres will provide information on the energy distribution of the incident neutrons. Provided an accurate knowledge of the energy dependence of the response of each sphere, $R_i(E)$ (where “ i ” indicates the sphere and E the neutron energy), an “unfolding” computer code is used to estimate the neutron spectrum. This is usually done by changing iteratively an initial “guess” spectrum, till the correspondent calculated Bonner sphere responses are in agreement with the measurements.

In this problem, a typical BSS is proposed. The sphere diameters are: 0” (bare detector), 2”, 3”, 5”, 8”, 10” and 12” with polyethylene density 0.950 g cm^{-3} . Such configuration allows getting spectral information from thermal to 20 MeV neutrons.

In order to extend the energy range up to hundreds of MeV, an additional lead loaded 12” sphere was also added. This new configuration takes advantage of the (n, xn) reactions induced by high energy neutrons in the lead shell. The structure of the new sphere includes a 8 cm diameter polyethylene sphere immediately around the central detector, surrounded by a 1 cm lead layer (two half shells), then polyethylene till an external diameter of 12”. Figure 1 shows the complete set, with internal details of the lead loaded sphere. Despite this sphere wouldn’t be strictly necessary for the neutron spectra proposed in the problem, it constitutes an interesting example of how the BSSs have been adapted to high energy fields.

A cylindrical 4 mm (diameter) x 4 mm (height) $^6\text{LiI(Eu)}$ (96% of ^6Li) active scintillator is used as central detector. Thermal neutrons are detected through the $^6\text{Li}(n,\alpha)^3\text{H}$ reaction (Q value = 4.78 MeV). The electronic pulses from the photomultiplier are counted by a scaler. The photon sensitivity of the detector is assumed to be negligible.

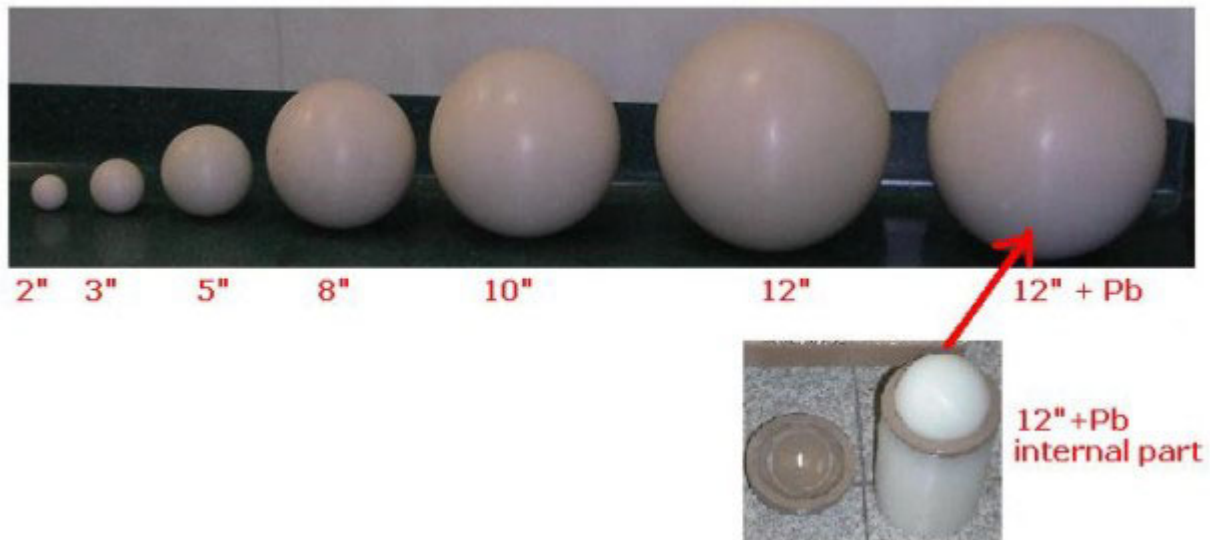


Figure 1. The set of spheres: 2”, 3”, 5”, 8”, 10”, 12” and 12”+Pb with details on the internal part.

Detector geometry and specifications

A cross sectional view of the central detector is shown in Figure 2. The whole assembly has a cylindrical geometry. The active part is labelled as “4x4 mm $^6\text{Li(Eu)}$ crystal”, and its center is located at 0.9 cm from the right external surface of the Aluminium assembly. All parts in grey are in aluminium. The not shadowed

parts can be considered in vacuum. The light pipe connecting the scintillator to the photomultiplier is in plexiglass.

The number of ${}^6\text{Li}(n,\alpha){}^3\text{H}$ reactions in the scintillator is assumed to be proportional to the number of pulses registered by the scaler.

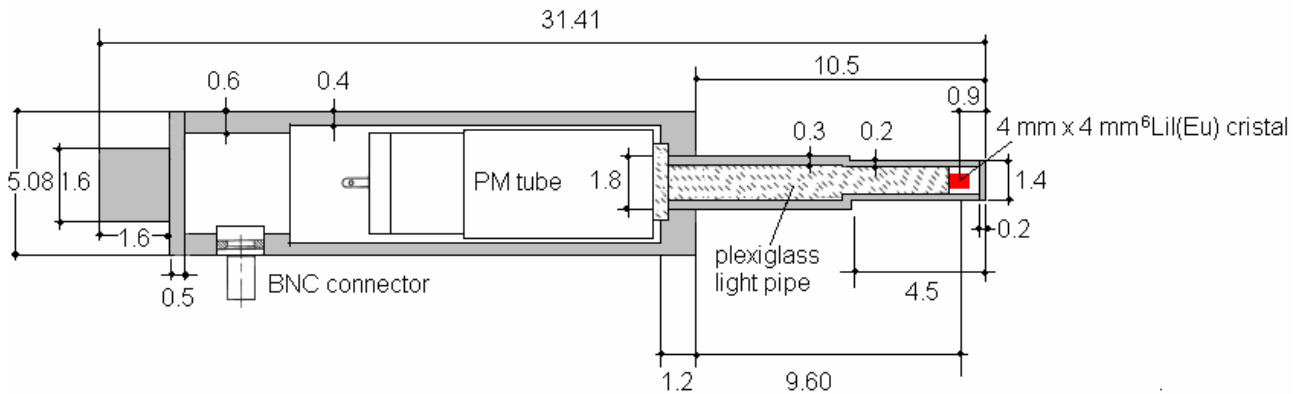


Figure 2. The central detector of the BSS. All dimensions are in cm.

Energy Spectra

Two ISO Reference Neutron Spectra are to be investigated, bare ${}^{252}\text{Cf}$ and ${}^{241}\text{Am-Be}$. According to the standard ISO 8529-1, the two spectra are listed in Table II as group source strengths, B_i , in certain energy intervals, i.e. the source strength of neutrons having energies between E_i and E_{i+1} .

In Figures 3 and 4, taken from the ISO specifications, the two spectra are represented as histogram plots of $dB_E/d(\ln E/E_0)$ (on a linear scale) versus the neutron energy, E_n (on a logarithmic scale).

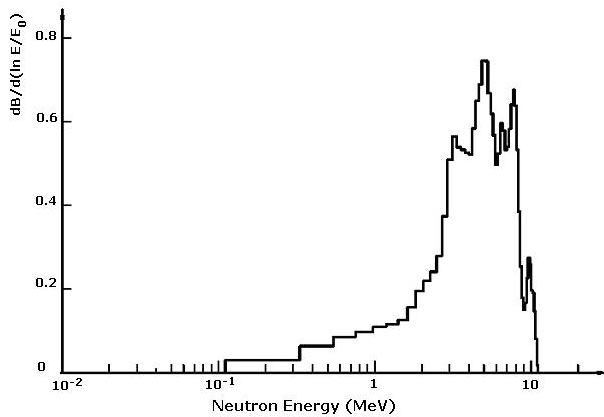


Figure 3. Equilethargic representation of the neutron spectrum from a ${}^{241}\text{Am-Be}(\alpha,n)$ source (ISO 8529-1). The area subtended by the curve is proportional to the neutron fluence

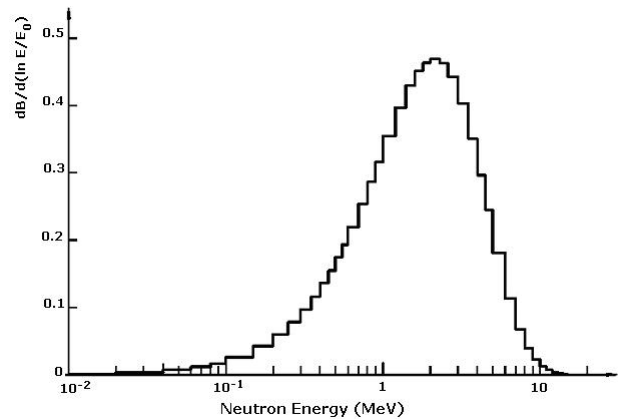


Figure 4. Equilethargic representation of the neutron spectrum from a ${}^{252}\text{Cf}$ spontaneous fission source (ISO 8529-1). The area subtended by the curve is proportional to the neutron fluence

Table II. Values of group source strength for the $^{241}\text{Am-Be}$ and ^{252}Cf sources

Reference ISO Neutron Spectra			
Am-Be		Cf (Bare)	
Energy (MeV)	Bi	Energy(MeV)	Bi
4.14E-07	1.44E-02	4.14E-07	3.10E-10
1.10E-01	3.34E-02	1.00E-06	1.11E-08
3.30E-01	3.13E-02	1.00E-05	1.27E-07
5.40E-01	2.81E-02	5.00E-05	2.76E-07
7.50E-01	2.50E-02	1.00E-04	7.82E-07
9.70E-01	2.14E-02	2.00E-04	2.21E-06
1.18E+00	1.98E-02	4.00E-04	4.53E-06
1.40E+00	1.75E-02	7.00E-04	5.68E-06
1.61E+00	1.92E-02	1.00E-03	5.51E-05
1.82E+00	2.23E-02	3.00E-03	1.28E-04
2.04E+00	2.15E-02	6.00E-03	2.30E-04
2.25E+00	2.25E-02	1.00E-02	7.74E-04
2.47E+00	2.28E-02	2.00E-02	2.17E-03
2.68E+00	2.95E-02	4.00E-02	2.80E-03
2.90E+00	3.56E-02	6.00E-02	3.29E-03
3.11E+00	3.69E-02	8.00E-02	3.68E-03
3.32E+00	3.46E-02	1.00E-01	1.05E-02
3.54E+00	3.07E-02	1.50E-01	1.21E-02
3.75E+00	3.00E-02	2.00E-01	1.33E-02
3.97E+00	2.69E-02	2.50E-01	1.42E-02
4.18E+00	2.86E-02	3.00E-01	1.49E-02
4.39E+00	3.18E-02	3.50E-01	1.55E-02
4.61E+00	3.07E-02	4.00E-01	1.60E-02
4.82E+00	3.33E-02	4.50E-01	1.63E-02
5.04E+00	3.04E-02	5.00E-01	1.66E-02
5.25E+00	2.74E-02	5.50E-01	1.68E-02
5.47E+00	2.33E-02	6.00E-01	3.38E-02
5.68E+00	2.06E-02	7.00E-01	3.39E-02
5.89E+00	1.82E-02	8.00E-01	3.37E-02
6.11E+00	1.77E-02	9.00E-01	3.33E-02
6.32E+00	2.04E-02	1.00E+00	6.46E-02
6.54E+00	1.83E-02	1.20E+00	6.12E-02
6.75E+00	1.63E-02	1.40E+00	5.73E-02
6.96E+00	1.68E-02	1.60E+00	5.31E-02
7.18E+00	1.68E-02	1.80E+00	4.88E-02
7.39E+00	1.88E-02	2.00E+00	6.55E-02
7.61E+00	1.84E-02	2.30E+00	5.67E-02
7.82E+00	1.69E-02	2.60E+00	6.33E-02
8.03E+00	1.44E-02	3.00E+00	6.21E-02
8.25E+00	9.68E-03	3.50E+00	4.68E-02
8.46E+00	6.52E-03	4.00E+00	3.49E-02
8.68E+00	4.26E-03	4.50E+00	2.58E-02
8.89E+00	3.67E-03	5.00E+00	3.30E-02
9.11E+00	3.81E-03	6.00E+00	1.74E-02
9.32E+00	5.06E-03	7.00E+00	9.01E-03
9.53E+00	6.25E-03	8.00E+00	4.61E-03
9.75E+00	5.52E-03	9.00E+00	2.33E-03
9.96E+00	4.68E-03	1.00E+01	1.17E-03
1.02E+01	3.70E-03	1.10E+01	5.83E-04
1.04E+01	2.78E-03	1.20E+01	2.88E-04
1.06E+01	1.51E-03	1.30E+01	1.42E-04
1.08E+01	3.63E-04	1.40E+01	6.94E-05

The problems

The results of this problem will be directly compared with experimental data obtained with the spectrometer under study exposed to $^{241}\text{Am-Be}$ and ^{252}Cf sources, using the shadow cone technique.

To meet the minimal requirements of the problem, items 1) and 2) are highly recommended, since the algorithms to infer the neutron spectrum rely on the change of the detector response due to changes in the diameter or composition of the sphere.

Item 3) is a valid exercise to check the simulation model, since the required energy dependence can be easily compared with reliable literature data [3].

Item 4) is interesting in order to complete the study on the variation of the detector response as the moderating assembly changes, evaluating the overall consistency of the simulation model.

Despite the knowledge of the neutron spectrum at the centre of the sphere is not mandatory for a good management of the Bonner Spheres technique, item 5) helps to clearly understand the “spectrum shifter” action of the polyethylene moderator. The study of both $^{241}\text{Am-Be}$ and ^{252}Cf sources will clearly indicate why the response of a given sphere changes as the incident neutron spectrum changes. All irradiations should be considered in vacuo.

1) **^{252}Cf source:** determine the response of the 2”, 3”, 8” and 10” spheres exposed to a parallel neutron beam of the same cross sectional area of the spheres. Expose all spheres with the detector axis parallel to the radiation field with the light pipe opposing the field direction. Normalize all results to the 8” sphere.

2) **$^{241}\text{Am-Be}$ source:** determine the response of the 5”, 8”, 10” and 12” spheres exposed to a parallel neutron beam of the same cross sectional area of the spheres. Expose all spheres with the detector axis parallel to the radiation field with the light pipe opposing the field direction. Normalize all results to the 8” sphere.

The following items should have the same geometry configuration as items 1 and 2.

3) Determine the response of the 8” sphere, exposed to a parallel neutron beam of the same cross sectional area of the sphere, for the following energies (expressed in MeV):

2.53E-8, 1.0E-6, 1.4663E-3, 1.1225E-2, 1.1225E-1, 5.6226E-1, 8.9107E-1, 1.411, 2.24, 4.4654, 17.776.

Plot the results normalized to the maximum value.

4) Determine the response of the 2” and 3” configurations to the $^{241}\text{Am-Be}$ (the “bare” configuration can be avoided, since the response will be insignificantly small). Considering the complete set of responses (2”, 3”, 5”, 8”, 10”, 12”), put the results in a table:

Column 1: sphere diameter in inches

Column 2: response normalized to the 8”.

5) For the 8” sphere exposed to $^{241}\text{Am-Be}$ and ^{252}Cf : determine the neutron spectrum within the inner thin lenticular layer (0.1 mm thick) inside the Bonner sphere towards the source and perpendicular to the beam axis. The energy binning reported in Table II (the higher limit of each interval is reported) should be adopted for this item:

Table II. Energy group structure proposed for the neutron spectra calculations. The energy values are logarithmically equidistant with five bins per decade.

Energy Boundaries (MeV)					
1.000E-09	6.310E-08	1.000E-06	1.000E-03	1.000E-01	3.162E+00
1.585E-09	7.586E-08	1.585E-06	1.585E-03	1.259E-01	3.981E+00
2.512E-09	9.120E-08	2.512E-06	2.512E-03	1.585E-01	5.012E+00
3.981E-09	1.096E-07	3.981E-06	3.981E-03	1.995E-01	6.310E+00
6.310E-09	1.318E-07	6.310E-06	6.310E-03	2.512E-01	7.943E+00
1.000E-08	1.585E-07	1.000E-05	1.000E-02	3.162E-01	1.000E+01
1.202E-08	1.905E-07	1.585E-05	1.259E-02	3.981E-01	1.259E+01
1.445E-08	2.291E-07	2.512E-05	1.585E-02	5.012E-01	1.585E+01
1.738E-08	2.754E-07	3.981E-05	1.995E-02	6.310E-01	2.000E+01
2.089E-08	3.311E-07	6.310E-05	2.512E-02	7.943E-01	
2.512E-08	3.981E-07	1.000E-04	3.162E-02	1.000E+00	
3.020E-08	4.786E-07	1.585E-04	3.981E-02	1.259E+00	
3.631E-08	5.754E-07	2.512E-04	5.012E-02	1.585E+00	
4.365E-08	6.918E-07	3.981E-04	6.310E-02	1.995E+00	
5.248E-08	8.318E-07	6.310E-04	7.943E-02	2.512E+00	

References

- [1] Bramblett, R. L., Ewing, R. I. and Bonner, T. W. *A new type of neutron spectrometer*. Nucl. Instr. Meth. **9**, 1-12 (1960).
- [2] International Standard ISO 8529. Reference neutron radiations – Part 1: *Characteristics and methods of production*. International Standard ISO 8529-1 (2001).
- [3] V. Mares and H. Schraube, “Evaluation of the response matrix of a Bonner sphere spectrometer with LiI detector from thermal energy to 100 MeV”, Nucl. Instr. and Meth. A **337**, 461-473 (1994).

ANNEX I

Material composition data

Material	Density (g cm-3)	Elemental composition (w%)
Lithium Iodide	3.494	⁶ Li= 4.36%, ⁷ Li= 0.18%, I=95.46%
PMMA (C ₅ H ₈ O ₂) _n	1.19	H=8%, C=60%, O=32%
Aluminum	2.7	Al=100%
Polyethylene (C ₂ H ₄) _n	0.95	C=85.7%, H=14.3%
Lead	11.35	Pb=100%

Problem proposed by:

G. Gualdrini ENEA-IRP Bologna Italy, R. Bedogni and A. Esposito INFN-LNF Frascati Italy

TO PRESERVE THE SCOPE OF THE COMPARISON ON THE EIGHT PROBLEMS, THE PARTICIPANTS ARE ASKED NOT TO PUBLISH THEIR RESULTS IN THE OPEN LITERATURE BEFORE THE FINAL WORKSHOP (AUTUMN 2007).

Correspondence:
Results should be returned to:
Gianfranco Gualdrini
ENEA- Istituto di Radioprotezione
Via dei Colli 16
40136 Bologna, Italy – guald@bologna.enea.it

P3- SIGMA SIMULATED WORKPLACE NEUTRON FIELD

Introduction

A thermal neutron energy-distribution is one of the fields recommended by the International Organization for Standardization (ISO, 2001) for determining the response of neutron measuring devices as a function of energy and for international intercomparisons of neutron fluence measurements. To assess the thermal neutron response of spectrometers, survey instruments and personal dosimeters, the “Institut de Radioprotection et de Sûreté Nucléaire” (IRSN) owns a thermal neutron facility called SIGMA (Figure 1), where the neutron field is produced by the moderation of fast neutrons emitted from six $^{241}\text{Am-Be}$ sources. A reference position, where calibrations are usually carried out, is defined at 50 cm from the moderating assembly. The neutron field at this calibration position has been newly characterized by experimental measurements and Monte Carlo simulations

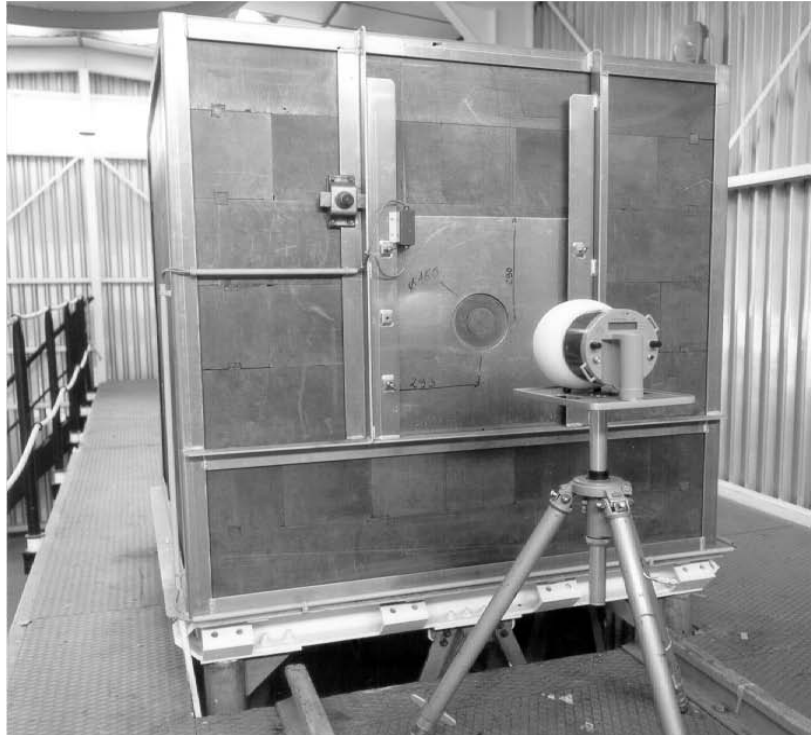


Figure 1. The SIGMA facility showing the graphite moderating block. A neutron survey instrument is placed at the reference position.

Task: model the field at the reference position.

Several sub-tasks are proposed but solutions that do not attempt all parts of the problem are most welcome. The computation is very demanding in terms of cpu, so you are advised to consider very carefully the computational techniques that you apply.

The tasks are not all rigidly specified. You should note the information given in the supplementary data section at the end of the problem specification. It is assumed that you will be able to work out the best means of determining the parameters of interest. There is more than one way of doing this for some tasks.

No recommendations for the tallying/scoring of the results are given: you will need to be aware of the precise definition of the quantity that they are being asked to calculate. Please explain exactly how you have scored the results when you report them. If this is not done interpretation of the results given will be very difficult. If you are not sure how to proceed with the calculations, or require some of the supplementary data in electronic format, please contact the author of the problem for assistance (rick.tanner@hpa.org.uk).

Description of the facility

The SIGMA facility was built to provide a thermal neutron field and the surrounding structures were designed to minimize the neutron background (Lacoste *et al*, 2004). The experimental hall is 6 m wide, 12 m long and 4.5 m high. To reduce the background coming from neutron scattering, the 5 cm thick walls comprise a glass-wool layer between two 2.5 mm thick aluminium plates and the base of the graphite moderator block is about 2 m above the concrete floor. The block is supported by metallic columns such that the base is 20 cm above a thin metallic platform.

The SIGMA assembly is constructed from high purity graphite, of density 1.70 g cm^{-3} , to moderate the fast neutrons from the six $0.6 \text{ TBq } ^{241}\text{Am-Be}$ sources. The dimensions of the block are $1.5 \times 1.5 \times 1.5 \text{ m}^3$. Six

horizontal channels, each 40 mm in diameter, are used to introduce the radioactive neutron sources and are located hexagonally around the centre of the block. Once the sources are introduced, the cylindrical channels are refilled with graphite. The sources are placed horizontally and the centre of each is about 25 cm from the centre of the graphite block. The six $^{241}\text{Am-Be}$ sources are sealed in a stainless steel cylindrical capsule with an external diameter of 35 mm and a height of 70 mm. The side walls of the capsule are 0.2038 cm thick whilst the top and bottom are 0.28575 cm thick. The emission rate of the sealed sources was measured using the manganese bath method in 1968. The total strength of the six sources was $(1.9071 \pm 0.0414) \times 10^8 \text{ n s}^{-1}$ in 4π when the recent reference spectrometry measurements were performed. The density of the AmO_2Be within the source capsule should be taken to be 1.12 g cm^{-3} . The simulated $^{241}\text{Am-Be}$ neutron fluence energy distribution to be used is that recommended by the International Organization for Standardization (Table 1).

Table 1. Probability (P_i) of a neutron being emitted with energy from E_i to E_{i+1} ($\sum P_i = 1$). This is the ISO energy distribution for the $^{241}\text{Am-Be}$ source.

i	E_i (MeV)	P_i	i	E_i (MeV)	P_i	i	E_i (MeV)	P_i
1	4.14E-07	1.44E-02	19	3.75E+00	3.00E-02	37	7.61E+00	1.84E-02
2	1.10E-01	3.34E-02	20	3.97E+00	2.69E-02	38	7.82E+00	1.69E-02
3	3.30E-01	3.13E-02	21	4.18E+00	2.86E-02	39	8.03E+00	1.44E-02
4	5.40E-01	2.81E-02	22	4.39E+00	3.18E-02	40	8.25E+00	9.68E-03
5	7.50E-01	2.50E-02	23	4.61E+00	3.07E-02	41	8.46E+00	6.52E-03
6	9.70E-01	2.14E-02	24	4.82E+00	3.33E-02	42	8.68E+00	4.26E-03
7	1.18E+00	1.98E-02	25	5.04E+00	3.04E-02	43	8.89E+00	3.67E-03
8	1.40E+00	1.75E-02	26	5.25E+00	2.74E-02	44	9.11E+00	3.81E-03
9	1.61E+00	1.92E-02	27	5.47E+00	2.33E-02	45	9.32E+00	5.06E-03
10	1.82E+00	2.23E-02	28	5.68E+00	2.06E-02	46	9.53E+00	6.25E-03
11	2.04E+00	2.15E-02	29	5.89E+00	1.82E-02	47	9.75E+00	5.52E-03
12	2.25E+00	2.25E-02	30	6.11E+00	1.77E-02	48	9.96E+00	4.68E-03
13	2.47E+00	2.28E-02	31	6.32E+00	2.04E-02	49	1.02E+01	3.70E-03
14	2.68E+00	2.95E-02	32	6.54E+00	1.83E-02	50	1.04E+01	2.78E-03
15	2.90E+00	3.56E-02	33	6.75E+00	1.63E-02	51	1.06E+01	1.51E-03
16	3.11E+00	3.69E-02	34	6.96E+00	1.68E-02	52	1.08E+01	3.63E-04
17	3.32E+00	3.46E-02	35	7.18E+00	1.68E-02	53	1.10E+01	0
18	3.54E+00	3.07E-02	36	7.39E+00	1.88E-02			

Geometric specification

- Assume that the $1.5 \times 1.5 \times 1.5 \text{ m}^3$ graphite block is centred at the origin in the following description and is of completely uniform composition, apart from the six $^{241}\text{Am-Be}$ sources contained within it.
- x -axis: runs horizontally through the centre of the graphite block towards the reference position. Positive x towards the reference position.
- y -axis: runs horizontally through the centre of the graphite block (determine positive y from x and z).
- z -axis: vertical. Positive z up.
- Reference position for calculation: (125 cm, 0, 0)
- The six sources are located according to the data given in Table 2. Their positions are depicted in Figure 2.

Table 2. Data for the geometric centre and emission rate of each of the sources.

Source	x (cm)	y (cm)	z (cm)	Emission rate (fraction)
1	-15.0	-10.5	+18.2	0.1591
2	+15.0	-21.0	0.0	0.1693
3	-15.0	-10.5	-18.2	0.1651
4	+15.0	+10.5	-18.2	0.1651
5	-15.0	+21.0	+0.0	0.1651
6	+15.0	+10.5	+18.2	0.1758

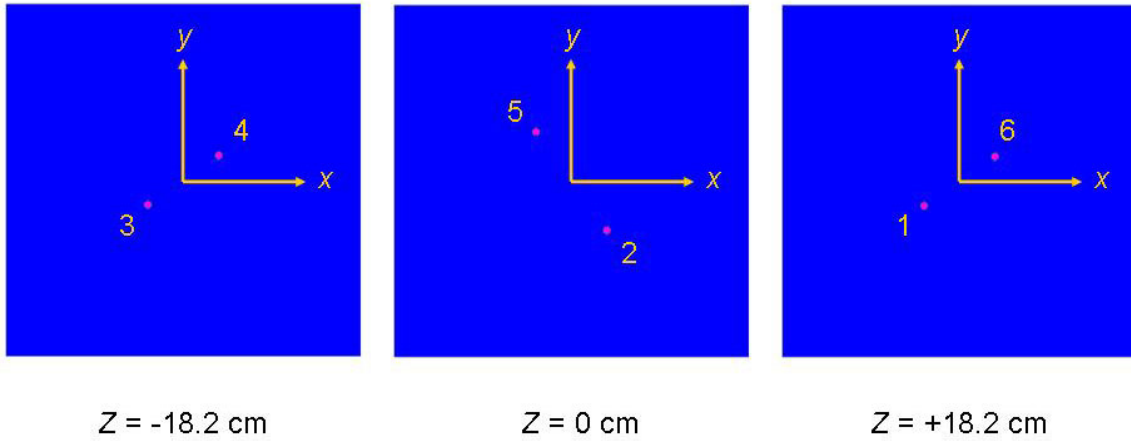


Figure 2. Positions of the six sources (●) inside the graphite block (blue) for three different horizontal slices.

- There is a metal platform around the graphite block to support experimental equipment and to allow scientists to walk around the facility. It is made from steel and is 0.6 cm thick. Its upper surface is 20 cm below the base of the graphite block. The planes that are used to define it are given in Table 3. There is a hole in the platform that has the same x-y dimensions as the external dimensions of the graphite block.
- The roof of the building and columns on which the graphite block is supported can be ignored.
- The floor of the building is made from 20 cm thick concrete.
- The walls of the building are made from a sandwich of glass wool between two 2.5 mm thick plates of aluminium. The glass wool can be ignored and the walls may be simulated using a 5 mm thick plate of aluminium. They are corrugated but you may assume them to be flat. The surfaces used to define the walls are given in Table 3.

Table 3. Planes used to define the platform for personnel to walk on and walls of the facility.

Wall	x_{min} (cm)	x_{max} (cm)	y_{min} (cm)	y_{max} (cm)	z_{min} (cm)	z_{max} (cm)
Platform	-640.0	560.0	-151.5	151.5	-95.6	-95.0
West wall	560.0	560.5	-448.5	151.5	-295.0	105.0
South wall	-640.0	560.0	151.5	152.0	-295.0	105.0
North wall	Do not simulate					
East wall	Do not simulate					
Roof	Do not simulate					

Materials

The material specifications to be used are given in Table 4.

Table 4. Material specifications to be used in the modelling.

Material	ρ (g cm ⁻³)	Element /isotope	Mass fraction	Material	ρ (g cm ⁻³)	Element	Mass fraction
Graphite	1.70	C	1.0	Concrete	2.289	Mg	5.670E-03
AmO ₂ Be	1.12	²⁴¹ Am	0.08			Mn	2.882E-04
		O	0.001			O	5.219E-01
		Be	0.909			Al	3.968E-02
Dry Air - ICRU 49 (ICRU, 1993a)	0.00120484	N	0.755267			Pb	2.016E-03
		O	0.231781			H	5.227E-03
		C	0.000124			Cl	3.352E-03
		Ar	0.012827			K	1.185E-02
Aluminium	2.70	Al	1.0			Si	2.779E-01
Steel	7.87	Fe	0.67145			Ca	1.130E-01
		Cr	0.185	Na	1.057E-02		
		Ni	0.1125	C	2.271E-03		
		Mn	0.02	Fe	6.260E-03		
		Si	0.01	ICRU Tissue (ICRU 1971; ICRU, 1993b)	H	0.101	
		P	0.00045		C	0.111	
		S	0.0003		N	0.026	
		C	0.0003		O	0.762	

Tasks

Additional information on the quantities can be found in the literature (Siebert and Schuhmacher, 1995; ICRU, 1971; ICRU, 1993a; ICRU, 1993b; ICRU, 1998a; ICRU 1998b; ICRU, 2001). If doubts persist please contact the author of this problem (rick.tanner@hpa.org.uk).

- Determine the fluence rate at the reference point.
- Determine the energy distribution at the reference point. Participants should use the energy bins provided in Table 5. It is important that all participants use the same energy bins since otherwise the solutions cannot easily be compared. If statistics are poor, participants may combine the bins given in Table 5 to give a coarser energy grid.
- Determine the $H^*(10)$ rate at the reference point.
- Determine the $H_p(10, 0^\circ)$ rate at the reference point taking 0° to be in a direction from the reference point to the centre of the moderating block.
- Determine the $H_p(10, 45^\circ)$ rate at the reference point taking 0° to be in a direction from the reference point to the centre of the moderating block.
- Calculate the component of the fluence at the reference point that is due to scatter from the walls, concrete floor and platform.
- Determine the sensitivity of the fluence at the reference point to the density of ²⁴¹AmO₂Be and graphite and examine whether there are other major sources of uncertainty associated with the fluence at the reference point. **Important note: the published data for this facility use a**

$^{241}\text{AmO}_2\text{Be}$ density of 0.207 g cm^{-3} . Participants can (optionally) investigate the same scenario using also the density of 0.207 g cm^{-3} (besides the 1.12 g cm^{-3} density stated in Table 4) to determine the influence of this on the results.

References

- International Commission on Radiation Units and Measurements (1971). Radiation quantities and units. ICRU Report 19 (Bethesda, MD: ICRU).
- International Commission on Radiation Units and Measurements (1993a). Stopping powers and ranges for protons and alpha particles. ICRU Report 49 (Bethesda, MD: ICRU).
- International Commission on Radiation Units and Measurements (1993b). Quantities and units in radiation protection dosimetry. ICRU Report 51 (Bethesda, MD: ICRU).
- International Commission on Radiation Units and Measurements (1998a). Conversion coefficients for use in radiological protection against external radiation. ICRU Report 57 (Bethesda, MD: ICRU).
- International Commission on Radiation Units and Measurements (1998b). Fundamental quantities and units for ionizing radiation. ICRU Report 60 (Bethesda, MD: ICRU).
- International Commission on Radiation Units and Measurements (2001). Determination of the operational dose equivalent quantities for neutrons. ICRU Report 66 (Bethesda, MD: ICRU).
- International Organization for Standardization (2001). Reference neutron radiations - Part 1: characteristics and methods of production. ISO 8529 10-1 (Geneva: ISO).
- Lacoste, V, Gressier, V, Muller, H and Lebreton L (2004). Characterisation of the IRSN graphite moderated Americium-beryllium neutron field. *Radiat Prot Dosim*, 110 (1-4), 135 10-139.
- NUMEC(1967). Americium Data Sheet, Nuclear Materials and Equipment Corporation, Technical Data Sheet, Apollo, Pennsylvania.
- Siebert, B R L and Schuhmacher, H (1995). Quality factors, ambient and personal dose equivalent for neutrons, based on the new ICRU stopping power data for protons and alpha particles. *Radiat Prot Dosim*, 58 (3), 177 10-183.

Supplementary information and data

The ICRU sphere is a 30 cm radius sphere composed of ICRU 4-element tissue (Table 4). The quantity $H^*(10)$ is defined in this sphere after the field has been expanded and aligned. It is calculated at a depth of 10 mm below the outer surface of the sphere on the axis that passes through the centre of the sphere that is parallel to the alignment of the field on the radius opposing the direction of the field.

The ICRU slab is a $30 \times 30 \times 15$ cm phantom in which it is convenient to define the quantity $H_p(10)$. It is composed of ICRU 4-element tissue (Table 4) with one of the large 30×30 cm surfaces being defined as “front”. The normal to that surface is defined to be 0° . Where necessary an angle of incidence, α , may be defined relative to this axis. Whilst this specific phantom is not a part of the definition of the quantity, it was used for the calculation of the ICRP/ICRU fluence to dose equivalent conversion coefficients for $H_p(10, \alpha)$ and can constitute a useful device for computing the quantity in a workplace scenario.

Table 4. Energy bins to be used for the reporting of energy distributions. If required, coarser bin structure may be obtained by merging some or all of the bins specified. This may be useful where statistics within individual bins are inadequate. If finer bin structure is warranted, the participant may divide some or all of the bins below, since this may improve the graphical representation of the results. However, to ease the analysis, it is important that the basic bin structure below is retained.

Energy Boundaries (MeV)					
1.000E-09	6.310E-08	1.000E-06	1.000E-03	1.000E-01	3.162E+00
1.585E-09	7.586E-08	1.585E-06	1.585E-03	1.259E-01	3.981E+00
2.512E-09	9.120E-08	2.512E-06	2.512E-03	1.585E-01	5.012E+00
3.981E-09	1.096E-07	3.981E-06	3.981E-03	1.995E-01	6.310E+00
6.310E-09	1.318E-07	6.310E-06	6.310E-03	2.512E-01	7.943E+00
1.000E-08	1.585E-07	1.000E-05	1.000E-02	3.162E-01	1.000E+01
1.202E-08	1.905E-07	1.585E-05	1.259E-02	3.981E-01	1.259E+01
1.445E-08	2.291E-07	2.512E-05	1.585E-02	5.012E-01	1.585E+01
1.738E-08	2.754E-07	3.981E-05	1.995E-02	6.310E-01	2.000E+01
2.089E-08	3.311E-07	6.310E-05	2.512E-02	7.943E-01	
2.512E-08	3.981E-07	1.000E-04	3.162E-02	1.000E+00	
3.020E-08	4.786E-07	1.585E-04	3.981E-02	1.259E+00	
3.631E-08	5.754E-07	2.512E-04	5.012E-02	1.585E+00	
4.365E-08	6.918E-07	3.981E-04	6.310E-02	1.995E+00	
5.248E-08	8.318E-07	6.310E-04	7.943E-02	2.512E+00	

Problem proposed by:

R.Tanner Health Protection Agency, U.K. and V. Lacoste IRSN Cadarache F

TO PRESERVE THE SCOPE OF THE COMPARISON ON THE EIGHT PROBLEMS, THE PARTICIPANTS ARE ASKED NOT TO PUBLISH THEIR RESULTS IN THE OPEN LITERATURE BEFORE THE FINAL WORKSHOP (AUTUMN 2007).

Correspondence:

Results should be returned to:

Rick Tanner

HPA Chilton, Didcot, Oxon OX11 0RG, UK –

rick.tanner@hpa-rp.org.uk

Table 5a. Fluence to dose equivalent conversion coefficients for ambient and personal dose equivalent

E_n (MeV)	$H^*(10)/\Phi$ (pSv/cm ²)	$H_p(10, 0^\circ)/\Phi$ (pSv/cm ²)	$H_p(10, 15^\circ)/\Phi$ (pSv/cm ²)	$H_p(10, 30^\circ)/\Phi$ (pSv/cm ²)	$H_p(10, 45^\circ)/\Phi$ (pSv/cm ²)	$H_p(10, 60^\circ)/\Phi$ (pSv/cm ²)	$H_p(10, 75^\circ)/\Phi$ (pSv/cm ²)
1.00E-09	6.60	8.19	7.64	6.57	4.23	2.61	1.13
1.00E-08	9.00	9.97	9.35	7.90	5.38	3.37	1.50
2.53E-08	10.6	11.4	10.6	9.11	6.61	4.04	1.73
1.00E-07	12.9	12.6	11.7	10.3	7.84	4.70	1.94
2.00E-07	13.5	13.5	12.6	11.1	8.73	5.21	2.12
5.00E-07	13.6	14.2	13.5	11.8	9.40	5.65	2.31
1.00E-06	13.3	14.4	13.9	12.0	9.56	5.82	2.40
2.00E-06	12.9	14.3	14.0	11.9	9.49	5.85	2.46
5.00E-06	12.0	13.8	13.9	11.5	9.11	5.71	2.48
1.00E-05	11.3	13.2	13.4	11.0	8.65	5.47	2.44
2.00E-05	10.6	12.4	12.6	10.4	8.10	5.14	2.35
5.00E-05	9.90	11.2	11.2	9.42	7.32	4.57	2.16
1.00E-04	9.40	10.3	9.85	8.64	6.74	4.10	1.99
2.00E-04	8.90	9.84	9.41	8.22	6.21	3.91	1.83
5.00E-04	8.30	9.34	8.66	7.66	5.67	3.58	1.68
1.00E-03	7.90	8.78	8.20	7.29	5.43	3.46	1.66
2.00E-03	7.70	8.72	8.22	7.27	5.43	3.46	1.67
5.00E-03	8.00	9.36	8.79	7.46	5.71	3.59	1.69
1.00E-02	10.5	11.2	10.8	9.18	7.09	4.32	1.77
2.00E-02	16.6	17.1	17.0	14.6	11.6	6.64	2.11
3.00E-02	23.7	24.9	24.1	21.3	16.7	9.81	2.85
5.00E-02	41.1	39.0	36	34.4	27.5	16.7	4.78
7.00E-02	60.0	59.0	55.8	52.6	42.9	27.3	8.10
1.00E-01	88.0	90.6	87.8	81.3	67.1	44.6	13.7
1.50E-01	132	139	137	126	106	73.3	24.2
2.00E-01	170	180	179	166	141	100	35.5
3.00E-01	233	246	244	232	201	149	58.5
5.00E-01	322	335	330	326	291	226	102
7.00E-01	375	386	379	382	348	279	139
9.00E-01	400	414	407	415	383	317	171
1.00E+00	416	422	416	426	395	332	180

Table 5b. Fluence to dose equivalent conversion coefficients for ambient and personal dose equivalent (continued)

E_n (MeV)	$H^*(10)/\Phi$ (pSv/cm ²)	$H_p(10, 0^\circ)/\Phi$ (pSv/cm ²)	$H_p(10, 15^\circ)/\Phi$ (pSv/cm ²)	$H_p(10, 30^\circ)/\Phi$ (pSv/cm ²)	$H_p(10, 45^\circ)/\Phi$ (pSv/cm ²)	$H_p(10, 60^\circ)/\Phi$ (pSv/cm ²)	$H_p(10, 75^\circ)/\Phi$ (pSv/cm ²)
1.00E+00	416	422	416	426	395	332	180
1.20E+00	425	433	427	440	412	355	210
2.00E+00	420	442	438	457	439	402	274
3.00E+00	412	431	429	449	440	412	306
4.00E+00	408	422	421	440	435	409	320
5.00E+00	405	420	418	437	435	409	331
6.00E+00	400	423	422	440	439	414	345
7.00E+00	405	432	432	449	448	425	361
8.00E+00	409	445	445	462	460	440	379
9.00E+00	420	461	462	478	476	458	399
1.00E+01	440	480	481	497	493	480	421
1.20E+01	480	517	519	536	529	523	464
1.40E+01	520	550	552	570	561	562	503
1.50E+01	540	564	565	584	575	579	520
1.60E+01	555	576	577	597	588	593	535
1.80E+01	570	595	593	617	609	615	561
2.00E+01	600	600	595	619	615	619	570
1.00E+00	416	422	416	426	395	332	180
1.20E+00	425	433	427	440	412	355	210
2.00E+00	420	442	438	457	439	402	274
3.00E+00	412	431	429	449	440	412	306
4.00E+00	408	422	421	440	435	409	320
5.00E+00	405	420	418	437	435	409	331
6.00E+00	400	423	422	440	439	414	345
7.00E+00	405	432	432	449	448	425	361
8.00E+00	409	445	445	462	460	440	379
9.00E+00	420	461	462	478	476	458	399
1.00E+01	440	480	481	497	493	480	421
1.20E+01	480	517	519	536	529	523	464
1.40E+01	520	550	552	570	561	562	503
1.50E+01	540	564	565	584	575	579	520
1.60E+01	555	576	577	597	588	593	535
1.80E+01	570	595	593	617	609	615	561
2.00E+01	600	600	595	619	615	619	570

Table 6. Average quality factor weighted kerma factors for ICRU 4-element tissue. These may be applied to the fluence at a point in ICRU tissue to obtain the dose equivalent at that location.

E_n (MeV)	$Q_n k_f$ (pSv cm ²)	E_n (MeV)	$Q_n k_f$ (pSv cm ²)	E_n (MeV)	$Q_n k_f$ (pSv cm ²)	E_n (MeV)	$Q_n k_f$ (pSv cm ²)
1.00 10 ⁻⁹	1.70 10 ¹	2.00 10 ⁻²	1.63 10 ¹	5.00 10 ⁻¹	2.99 10 ²	3.50 10 ⁰	3.88 10 ²
1.58 10 ⁻⁹	1.35 10 ¹	3.60 10 ⁻²	3.54 10 ¹	5.40 10 ⁻¹	3.05 10 ²	3.70 10 ⁰	3.89 10 ²
2.51 10 ⁻⁹	1.07 10 ¹	6.30 10 ⁻²	6.96 10 ¹	5.80 10 ⁻¹	3.10 10 ²	3.90 10 ⁰	3.60 10 ²
3.98 10 ⁻⁹	8.50 10 ⁰	8.20 10 ⁻²	9.29 10 ¹	6.20 10 ⁻¹	3.16 10 ²	4.20 10 ⁰	3.62 10 ²
6.32 10 ⁻⁹	6.75 10 ⁰	8.60 10 ⁻²	9.72 10 ¹	6.60 10 ⁻¹	3.22 10 ²	4.60 10 ⁰	3.33 10 ²
1.00 10 ⁻⁸	5.36 10 ⁰	9.00 10 ⁻²	1.02 10 ²	7.00 10 ⁻¹	3.27 10 ²	5.00 10 ⁰	3.52 10 ²
2.53 10 ⁻⁸	3.37 10 ⁰	9.40 10 ⁻²	1.06 10 ²	7.40 10 ⁻¹	3.31 10 ²	5.40 10 ⁰	3.03 10 ²
3.60 10 ⁻⁸	2.86 10 ⁰	9.80 10 ⁻²	1.11 10 ²	7.80 10 ⁻¹	3.36 10 ²	5.80 10 ⁰	3.18 10 ²
6.30 10 ⁻⁸	2.16 10 ⁰	1.05 10 ⁻¹	1.18 10 ²	8.20 10 ⁻¹	3.39 10 ²	6.20 10 ⁰	3.18 10 ²
1.10 10 ⁻⁷	1.63 10 ⁰	1.15 10 ⁻¹	1.29 10 ²	8.60 10 ⁻¹	3.43 10 ²	6.60 10 ⁰	3.30 10 ²
2.00 10 ⁻⁷	1.21 10 ⁰	1.25 10 ⁻¹	1.38 10 ²	9.00 10 ⁻¹	3.50 10 ²	7.00 10 ⁰	3.50 10 ²
3.60 10 ⁻⁷	9.05 10 ⁻¹	1.35 10 ⁻¹	1.48 10 ²	9.40 10 ⁻¹	3.64 10 ²	7.40 10 ⁰	3.85 10 ²
6.30 10 ⁻⁷	6.85 10 ⁻¹	1.45 10 ⁻¹	1.57 10 ²	9.80 10 ⁻¹	3.93 10 ²	7.80 10 ⁰	3.49 10 ²
1.10 10 ⁻⁶	5.17 10 ⁻¹	1.55 10 ⁻¹	1.65 10 ²	1.05 10 ⁰	3.87 10 ²	8.20 10 ⁰	3.30 10 ²
2.00 10 ⁻⁶	3.84 10 ⁻¹	1.65 10 ⁻¹	1.73 10 ²	1.15 10 ⁰	3.66 10 ²	8.60 10 ⁰	3.51 10 ²
3.60 10 ⁻⁶	2.87 10 ⁻¹	1.75 10 ⁻¹	1.80 10 ²	1.25 10 ⁰	3.70 10 ²	9.00 10 ⁰	3.60 10 ²
6.30 10 ⁻⁶	2.17 10 ⁻¹	1.85 10 ⁻¹	1.88 10 ²	1.35 10 ⁰	3.71 10 ²	9.40 10 ⁰	3.57 10 ²
1.10 10 ⁻⁵	1.65 10 ⁻¹	1.95 10 ⁻¹	1.94 10 ²	1.45 10 ⁰	3.64 10 ²	9.80 10 ⁰	3.73 10 ²
2.00 10 ⁻⁵	1.24 10 ⁻¹	2.10 10 ⁻¹	2.04 10 ²	1.55 10 ⁰	3.64 10 ²	1.05 10 ¹	3.84 10 ²
3.60 10 ⁻⁵	9.47 10 ⁻²	2.30 10 ⁻¹	2.16 10 ²	1.65 10 ⁰	3.70 10 ²	1.15 10 ¹	4.41 10 ²
6.30 10 ⁻⁵	7.61 10 ⁻²	2.50 10 ⁻¹	2.26 10 ²	1.75 10 ⁰	3.63 10 ²	1.25 10 ¹	4.25 10 ²
1.10 10 ⁻⁴	6.73 10 ⁻²	2.70 10 ⁻¹	2.37 10 ²	1.85 10 ⁰	3.71 10 ²	1.35 10 ¹	4.56 10 ²
2.00 10 ⁻⁴	7.26 10 ⁻²	2.90 10 ⁻¹	2.45 10 ²	1.95 10 ⁰	3.61 10 ²	1.45 10 ¹	4.94 10 ²
3.60 10 ⁻⁴	1.03 10 ⁻¹	3.10 10 ⁻¹	2.55 10 ²	2.10 10 ⁰	3.58 10 ²	1.55 10 ¹	5.15 10 ²
6.30 10 ⁻⁴	1.75 10 ⁻¹	3.30 10 ⁻¹	2.61 10 ²	2.30 10 ⁰	3.41 10 ²	1.65 10 ¹	5.15 10 ²
1.10 10 ⁻³	3.30 10 ⁻¹	3.50 10 ⁻¹	2.71 10 ²	2.50 10 ⁰	3.41 10 ²	1.75 10 ¹	5.20 10 ²
2.00 10 ⁻³	6.90 10 ⁻¹	3.70 10 ⁻¹	2.79 10 ²	2.70 10 ⁰	3.45 10 ²	1.85 10 ¹	5.30 10 ²
3.60 10 ⁻³	1.50 10 ⁰	3.90 10 ⁻¹	2.90 10 ²	2.90 10 ⁰	3.48 10 ²	1.95 10 ¹	5.39 10 ²
6.30 10 ⁻³	3.23 10 ⁰	4.20 10 ⁻¹	3.14 10 ²	3.10 10 ⁰	3.53 10 ²	2.05 10 ¹	5.39 10 ²
1.10 10 ⁻²	7.01 10 ⁰	4.60 10 ⁻¹	3.13 10 ²	3.30 10 ⁰	3.91 10 ²		

Class 2 Problems

Expressing the overall uncertainties

P4 - PHOTON IRRADIATION FACILITY

Introduction

The problem is aimed at studying the uncertainty budget associated with the air kerma delivered by a simplified calibration beam which could be used for radiotherapy and radiation protection. It is only mandatory to answer question 1 compared with the uncertainty budget study. Questions 2 to 4 are given in order to help you in understanding and quantifying the influence of the calibration facility components. It is not mandatory to answer questions 2 to 4. The design of the irradiator is based on the specifications of ISO 4037 part 1, it is similar to those used in standard and accredited laboratories.

Source geometry

A point source and a volume source (cylindrical shaped) are proposed. The isotope is ^{137}Cs .

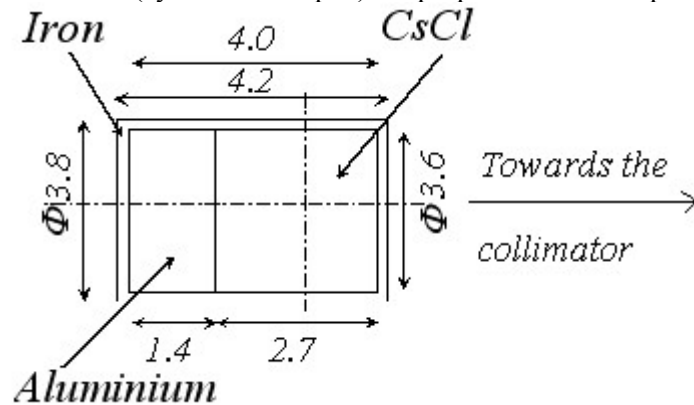


Figure 1: ^{137}Cs source. All dimensions are given in cm.

The source consists of a cylindrical pellet of CsCl (density: 4.00 g/cm^3). The core encapsulation is made of iron (density: 7.87 g/cm^3) 0.1 cm thick. The top is made of aluminium (density: 2.70 g/cm^3)

Table 1: Isotopic composition of the source materials normalised to 100%.

	Cs	Cl	Fe	Al
CsCl	50	50	-	-
Iron	-	-	100	-
Aluminium	-	-	-	100

Decay data ^{137}Cs : (absolute intensities are given between brackets), it is recommended to simulate only the gamma ray.

- Electrons: 324.2 keV (7.6%), 655.7 keV (1.4%), 660.3 keV (0.3%)
- Betas (Max Energy): 511.5 keV (94.6%), 1173.2 keV (5.4%)
- X rays: 31.8 keV (1.9%), 32.2 keV (3.6%), 36.3 keV (1.0%)
- Gamma ray: 661.66 keV (85.2%)

Table 2 : Conversion coefficients for air kerma per unit fluence K_a/Φ , for monoenergetic photons (ICRU 57)

E (MeV)	K_a/Φ (pGy.cm ²)	E (MeV)	K_a/Φ (pGy.cm ²)	E (MeV)	K_a/Φ (pGy.cm ²)	E (MeV)	K_a/Φ (pGy.cm ²)	E (MeV)	K_a/Φ (pGy.cm ²)
0.010	7.43	0.050	0.323	0.200	0.856	0.800	3.69	4.000	12.1
0.015	3.12	0.060	0.289	0.300	1.38	1.000	4.47	5.000	14.1
0.020	1.68	0.080	0.307	0.400	1.89	1.500	6.14	6.000	16.1
0.030	0.721	0.100	0.371	0.500	2.38	2.000	7.55	8.000	20.1
0.040	0.429	0.150	0.599	0.600	2.84	3.000	9.96	10.000	24.0

Irradiator geometry

The irradiator has a cylindrical symmetry and it is composed of two parts. The main timbering and the collimator are made of lead and tungsten alloy, respectively. Figure 2 shows the geometry.

Table 2: Isotopic composition of the irradiator materials.

	C	O	N	Ar	Ni	Cu	Pb	W
Dry Air (Wt Frac.) *	0.0124	23.1781	75.5267	1.2827	-	-	-	-
Tungsten alloy (At Frac) **	-	-	-	-	6.0	4.0	-	90.0
Lead (At Frac)+	-	-	-	-	-	-	100	-

* For dry air, data come from ICRU 49, the density is $1.20484 \times 10^{-3} \text{ g/cm}^3$

** The density of Tungsten alloy is 16.9 g/cm^3

+ The density of Pb is 11.34 g/cm^3

Detection points and quantities

The detection point is defined at 50 cm from the source (in case a point source is not used, the origin is taken from the centre of the radioactive core) along the axis of the irradiator.

The quantities of interest are the spectral fluence distribution and the total air kerma. In addition to that, the air kerma profile at 50 cm is required for evaluating field size penumbra.

Result will be normalized to one history; additionally results can be given per becquerel.

For the spectral fluence distribution, 133 bins are needed; the width of each bin being 5 keV.

The problem

Question 1 (mandatory):

This is the only mandatory question in this problem. Figure 2 presents the reference geometry for the overall problem; it includes all the features of the irradiation facility (source, lead shielding and collimator). See figure 1 for a detailed description of the source. This question is aimed at providing an uncertainty analysis of the calculation of the “reference” value of the air kerma at 50 cm from the centre of the source.

Calculate the air kerma and its uncertainty budget at 50 cm from the source (see figure 2 for irradiator geometry and figure 1 for source geometry).

The proposed approach to compute the uncertainty budget is to vary one parameter at a time. It is advised to enlarge the variation of the parameters to achieve reliable results, then to calculate the variation of the result corresponding to the uncertainty of the parameters under the assumption that the variation is linear (See table 3) and that the correlation between parameters is negligible. Finally, it is advised to apply the method of summing in quadrature the errors of every parameter to calculate the combined uncertainty (assuming no correlation between parameters). The variations of the parameters for the calculations are proposed in table 3 but it is up to the participant to modify them depending on the magnitude of the encountered variation in air kerma.

The method described above is only a proposal; participants are free to use a different method to estimate the standard uncertainty in terms of air kerma. The applied method should be described in order to enable the problem authors to compare the results. Table 3 gives a list of parameters that participants have to vary.

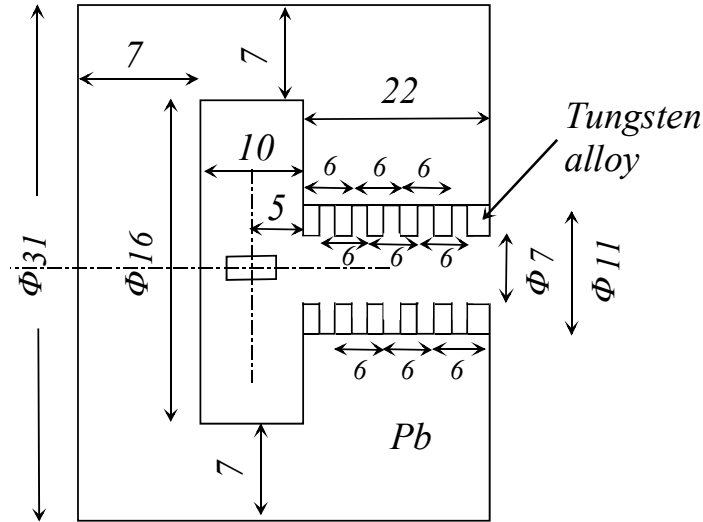


Figure 2: Cut view of the irradiator, all dimensions are given in cm, there is no wall around the irradiator. This scheme represents the geometry of reference. Each ring of the collimator (in tungsten alloy) is 2 cm thick.

Table 3: Example for the presentation of the results

Parameter identification X	Parameter variation in the calculation			Reported uncertainty in parameters (4)	Standard uncertainty of experimental parameter	
	ΔX	$\left(\frac{\partial k_{\text{air}}}{\partial x}\right)$	$\left(\frac{\partial k_{\text{air}}}{\partial x}\right) \Delta X$		u (5)	Δk_{air}
Position of the source (throw off centre)	$+(\Delta X)$ (1)	(2)	CC mGy (3)	+0.05 cm	$0.05 / 2\sqrt{3}$	$\frac{CC}{\Delta X} u$ (6)
Source chamber (depth)	$\pm(\Delta X/2)$			± 0.2 cm	$0.4 / 2\sqrt{3}$	
Rings collimator (diameter)	$\pm(\Delta X/2)$			± 0.05 cm	$0.1 / 2\sqrt{3}$	
tungsten alloy density	$\pm(\Delta X/2)$			± 0.2 g/cc	$0.4 / 2\sqrt{3}$	
Density of CsCL	$\pm(\Delta X/2)$			± 0.2 g/cc	$0.4 / 2\sqrt{3}$	

(1) Variation of the parameter in the calculation. For example if one decides to vary the location of the source of ± 0.5 cm around its nominal position, one has to write ± 0.5 cm in the column

(2) Prior to the calculation for column 3, participants have to determine the sensitivity $\partial k_{\text{air}} / \partial x$ using MC calculations. (the figures in the table are given as guide values for 10^{-20} Gy per history)

(3) $\Delta_K = |K_{(-\Delta X/2)} - K_{(+\Delta X/2)}|$ is the deviation between the results in terms of air kerma for calculations with the source located at $(-\Delta X/2)$, $K_{(-\Delta X/2)}$, and at $(+\Delta X/2)$, $K_{(+\Delta X/2)}$, from its nominal position. Participants have to account for the precision of the MC calculation u_{MC} . The following requirement must be fulfilled:

$$u_{MC} / \Delta_K < 0.1$$

To fulfil this condition, participants could enlarge ΔX or improve the precision of the MC calculations for example by increasing the number of histories. Whether this condition is not fulfilled, the participant should indicate the achieved ratio.

(4) Uncertainty on the parameter taken from literature, log books, schemes, ...

(5) The relation between column 4 and 5 depends on the shape of the distribution and the coverage factor of the original data. For a Gaussian distribution: $u = (\text{column 4}) / 6$, for a rectangular distribution: $u = (\text{column 4}) / 2\sqrt{3}$, whether the uncertainty on the parameter is reported for 3 standard deviations. See ISO 13005 for details.

(6) Uncertainty in term of air kerma normalized to the standard uncertainty value.

In addition to the parameters listed in table 3, it is up to you to add parameters to vary. Hereafter table 4 provides a non exhaustive list of additional parameters. It is up to the participant to select or not some parameters in the table, these parameters are not mandatory.

Table 4 : list of additional parameters (not mandatory)

Parameter identification X	Parameter variation in the calculation		Reported uncertainty in parameters (4)	Standard uncertainty of experimental parameter	
	ΔX	$(\partial k_{\text{air}} / \partial X)$		u (5)	Δk_{air}
Position of the source (depth)			+/-0.1 cm	$0.2 / 2\sqrt{3}$	
Source chamber (diameter)			+/-0.05 cm	$0.1 / 2\sqrt{3}$	
Length of the rings of the collimator			+/-0.05 cm	$0.1 / 2\sqrt{3}$	
Density of aluminium			+/-0.05 g/ cm ³	$0.1 / 2\sqrt{3}$	
Density of iron			+/-0.05 g/ cm ³	$0.1 / 2\sqrt{3}$	
Density of Lead			+/-0.1 g/ cm ³	$0.2 / 2\sqrt{3}$	
Energy cut off *					
Cross section and physics models *					

* Parameter which could introduce a bias in calculation

Question 2:

Influence of the source encapsulation (see figure 3 for the geometry)

This question is not mandatory but is recommended because in many circumstances one makes the assumption of a point source. It can be seen from the results to this question that this assumption is somewhat questionable.

Quantities:

- air kerma ; spectral fluence distribution ; air kerma profile

Calculate the air kerma and the spectral fluence distribution at 50 cm from the source.

Calculate the air kerma profile at 50 cm from the source.

The source is inside the irradiator, there is no wall around the facility.

a - Point source

b - Volume source without material (no self absorption) and without encapsulation

c - Volume source with material (to account for self absorption) but without encapsulation

d - Volume source with material (to account for self absorption) and with encapsulation

For geometries (b) to (d) the centre of the active part of the source is positioned at the place of the point source in geometry (a) (see figure 3).

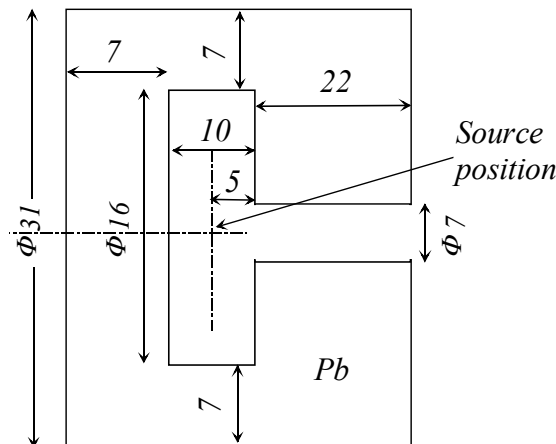


Figure 3: Cut view of the irradiator; the source is a point or a cylinder; all dimensions are given in cm; there is no wall around the irradiator.

Question 3: influence of the collimator (see figures 4a to 4d and figure 2)

This question is not mandatory. Five geometries (figures 4a, 4d and figure 3) are proposed. They allow to study the collimator influence by adding it progressively (in 5 steps). Whether you decide to make these calculations, it is recommended to calculate in priority the configurations corresponding to figure 4b and 4d.

Quantities: spectral fluence distribution; air kerma, air kerma profile

Calculate the air kerma and the spectral fluence distribution at 50 cm and 100 cm from the source.
Calculate the air kerma profile at 50 cm the source.

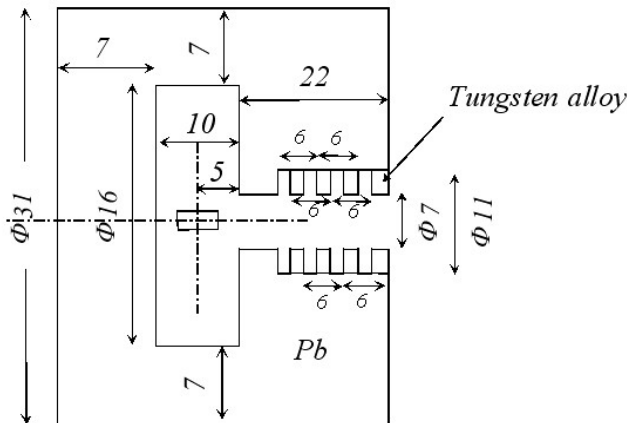


Figure 4a: Cut view of the irradiator, all dimensions are given in cm, there is no wall around the irradiator

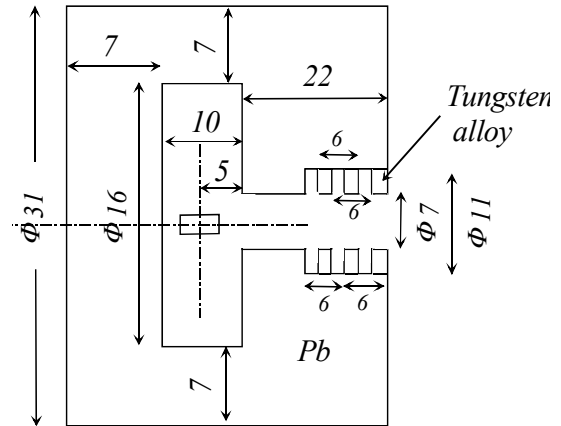


Figure 4b: Cut view of the irradiator, all dimensions are given in cm, there is no wall around the irradiator

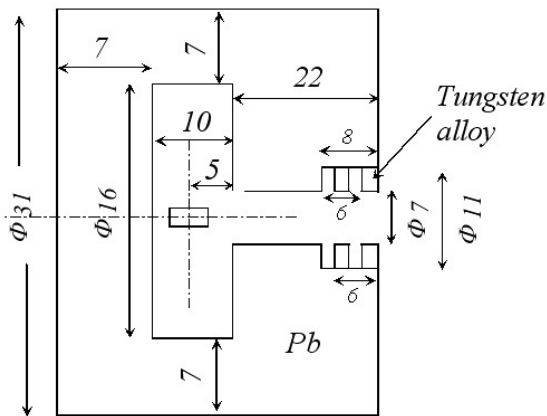


Figure 4c: Cut view of the irradiator, all dimensions are given in cm, there is no wall around the irradiator

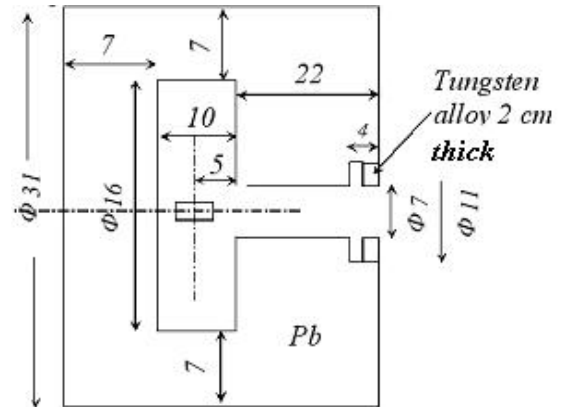


Figure 4d: Cut view of the irradiator, all dimensions are given in cm, there is no wall around the irradiator

Question 4: influence of the source chamber dimensions (see figure 5)

As question 2 and 3, this question is not mandatory.

Quantities:

- air kerma
- spectral fluence distribution

Calculate the air kerma and the spectral fluence distribution at 50 cm from the source.

Comparing results of question 3 and 4 put into evidence the influence of the source chamber dimensions.

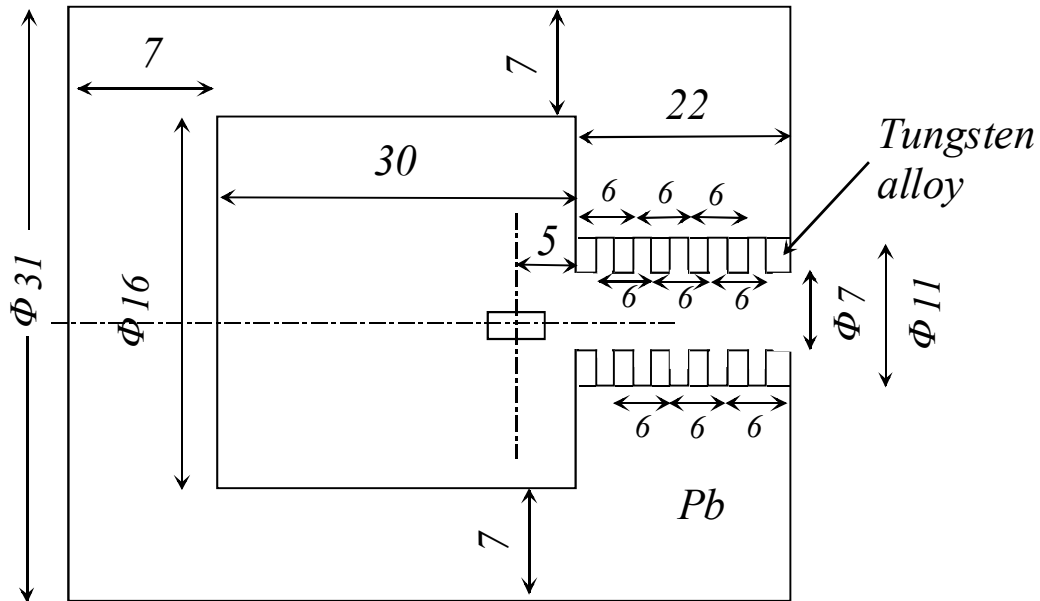


Figure 5: Cut view of the irradiator, all dimensions are given in cm, there is no wall around the irradiator

Problem proposed by:

Jean Marc Bordy CEA Saclay F, Christian Hranitzky ARCS Siebersdorf A, Helmut Vincke CERN Geneva CH

TO PRESERVE THE SCOPE OF THE COMPARISON ON THE EIGHT PROBLEMS, THE PARTICIPANTS ARE ASKED NOT TO PUBLISH THEIR RESULTS IN THE OPEN LITERATURE BEFORE THE FINAL WORKSHOP (AUTUMN 2007).

Correspondence:

Results should be returned to:

Jean Marc Bordy

CEA / DRT – LIST DETECS - LNHB – LMD

Bât. 534

Point courrier numéro 104

91191 Gif sur Yvette CEDEX FRANCE

jean-marc.bordy@cea.fr

Introduction

The neutron emission rate of radionuclide neutron sources is measured using the manganese bath technique: the source is immersed in a solution of manganese sulphate and the measured quantity, the *total neutron emission rate into 4π sr*, is derived from the ^{56}Mn activity produced by neutron activation of ^{55}Mn atoms. The neutrons emitted by the source, also interact with other nuclei such as H, O, S, impurities, and the magnitude of these “losses” has to be determined either by calculation or measurement.

Principle of the manganese bath technique

The neutron source to be calibrated in terms of total emission rate is placed at the centre of a spherical tank filled with an aqueous solution of manganese sulphate. The composition of the solution is accurately known allowing the determination of the hydrogen to manganese atom ratio, $N_{\text{H}}/N_{\text{Mn}}$. For a 1-meter diameter tank, an almost complete absorption of neutrons emitted by the source is achieved, but the “useful” reaction, i.e. the capture of source neutrons by manganese nuclei, is dealing with approximately 50% of emitted neutrons.

The ^{56}Mn radionuclides are created in the manganese bath by an (n,γ) reaction on ^{55}Mn . The ^{56}Mn nucleus decays through seven β^- transitions towards excited levels of ^{56}Fe with a half-life of 2.57878 (46) hours. The activity of the solution reaches an equilibrium state when the rate of creation of ^{56}Mn atoms by neutron activation is equal to the rate of radioactive disintegrations of ^{56}Mn . Other longer half-life radionuclides like ^{32}P and ^{35}S may also be created in the solution by activation of sulphur isotopes. The isotopic composition of natural sulphur is given in Table 1 of Appendix 2.

Various methods can be used for the measurement of the activity of the solution:

- Global counting by immersion of a NaI(Tl) detector after removal of the source.
- Activity measurement by a gamma-ray detector placed in a loop outside of the manganese bath sphere.
- Activity measurement of an aliquot of the solution by Liquid Scintillation Counting, by Cerenkov counting or by $4\pi\beta\text{-}\gamma$ coincidence-counting techniques.

If a neutron source is immersed in the bath, the variation of the number of ^{56}Mn atoms in the solution is due to two terms:

1. Creation of ^{56}Mn by (n,γ) reaction on ^{55}Mn .
2. Radioactive decay of ^{56}Mn .

The first term is proportional to the neutron emission rate of the source and the second term is proportional to the number of ^{56}Mn atoms in the solution as shown in equation (1):

$$\frac{dN}{dt} = \alpha B - \lambda N \quad (1)$$

where N is the number of ^{56}Mn atoms in the solution, α is the average probability of creation of ^{56}Mn per neutron emitted by the source, B is the neutron emission rate of the source and λ is the radioactive decay constant of ^{56}Mn . When the creation rate of ^{56}Mn equals its decay rate, dN/dt equals zero and equilibrium is reached (the saturation of the bath).

$$\frac{dN}{dt} \equiv 0 \rightarrow \alpha B = \lambda N \quad (2)$$

where λN is the total ^{56}Mn activity of the bath (number of disintegrations per time unit). The term α depends on the fraction of neutrons captured by ^{55}Mn over those captured by other nuclei and also on some corrective terms including neutron leakage and neutrons absorbed by the source material and the source container. Taking $\alpha = f(1-\delta)$, the neutron emission rate of the source (B) is linked to the ^{56}Mn activity per unit of mass of the manganese bath at saturation (A_m) through the following relation:

$$B = \frac{A_m M}{f(1 - \delta)} \quad (3)$$

Where:

- A_m : equilibrium activity per unit of mass of ^{56}Mn in the solution,
- M : total mass of manganese sulphate solution in the tank,
- f : fraction of neutrons captured by Mn nuclei over those captured by other nuclei (hydrogen, sulphur, ...),
- δ : correction factor: $(O + S + L)$ taking into account other neutron interactions as detailed below:
 - o O : fraction of source neutrons undergoing (n,α) reactions in oxygen, and (n,α) and (n,p) reactions in sulphur of the MnSO_4 solution.
 - o S : fraction of the source neutrons “recaptured” in the neutron source and the source cavity assembly.
 - o L : fraction of the source neutrons escaping from the solution tank.

In the experimental conditions described in this exercise, the value of f , function of the concentration of the solution, is about 0.5 and the correction factor is a few percent.

Other radionuclides can also be produced by activation in the solution: for example ^{32}P by (n,p) reaction on ^{32}S and ^{35}S by (n,γ) reaction on ^{34}S . These two radionuclides decay by pure-beta transition with half-lives of 14.284 (36) days and 87.32 (16) days respectively.

This problem is dedicated to the calculation of f , O , S and L and their associated uncertainties. The experimental validation of the calculation will be achieved using a reference (AmBe) neutron source, by measurements of the neutron leakage (L) and the equilibrium ^{56}Mn activity. The possibility of measurement of sulphur activation products, as ^{32}P and ^{35}S , will be also considered.

Consequently, this problem is expected to combine two complementary features: calculations and experiments. The calculations are necessary to determine the correcting factors due to interactions of source neutrons with “non-Mn” nuclei in the manganese sulphate bath and materials in the vicinity of the source to be calibrated (PMMA holder, source capsule, steel rods, etc.). It should be mentioned that the reliability of the calculated results is strongly dependent on the knowledge of the code input data (dimensions, material composition, cross-sections, etc.). The measurements of the neutron leakage from the boundaries of the tank and the contribution of neutrons scattered by the environment of the set-up require a detailed uncertainty analysis before comparison with calculated results.

Models of the facility

The calculation is proposed in two parts. In the first one, a simplified set-up is considered: a neutron point source immersed in a spherical manganese bath, installed in infinite vacuum. In the second one, a more realistic model is used, taking into account the geometrical description of a real source in its holder and the metallic manganese bath container. Optional description of the environment around the facility can also be taken into account in this second part. The purpose of the first part is mainly to compare the probability of activation of ^{55}Mn and the probability of neutron leakage in the case of a simplified model in order to deduce the influence of neutron interaction cross sections on the results without the interference of various other possible factors. It should be noticed that this simple geometry can also be dealt with deterministic codes, and, in addition, it is also expected to be helpful for the analysis of results derived from calculations performed with a more realistic one, when discrepancies between both sets of results are found.

Part 1, simplified model - Geometrical description

A point source (no dimensions) is placed at the centre of a spherical (radius 50 cm) manganese sulphate bath with the composition listed in Table 2 of Appendix 2.

The neutron spectrum is assumed to fit the (AmBe) energy distribution as recommended by the ISO 8529-1 Standard (2001) with an isotropic distribution (c.f. Appendix 3).

The manganese bath is located, without any container, in infinite vacuum.

Part 1, simplified model - Proposed tasks

The following tasks are proposed in which *all results should be normalised per neutron emitted from the point source*.

1. Calculation of the neutron fraction captured in the manganese sulphate solution.
2. Calculation of the neutron fraction captured by Mn of the bath solution [(n, γ) interactions]
3. Calculation of the neutron fraction captured by S isotopes [(n, γ), (n,p), (n, α), total interactions]
4. Calculation of the neutron fraction captured by O [(n, α) interactions]
5. Calculation of the neutron fraction captured by H [(n, γ) interactions]
6. Calculation of the fraction of neutrons escaping from the bath. A concentric spherical surface (radius = 70 cm) will be considered for that purpose and the neutron contribution will be evaluated on that surface.
7. Calculation of the neutron fluence spectrum on the same spherical surface Detailed energy binning of the neutron distributions and their graphical representation are given in Appendix 3.

Part 2, realistic model - Geometrical description

Sketches of the realistic model are displayed in Figures 1 and 2. Figure 1 represents the spherical tank (outer radius 50.00 cm; inner radius 49.75 cm), made of stainless steel 316 L. The chemical compositions of the components are given in Appendix 2.

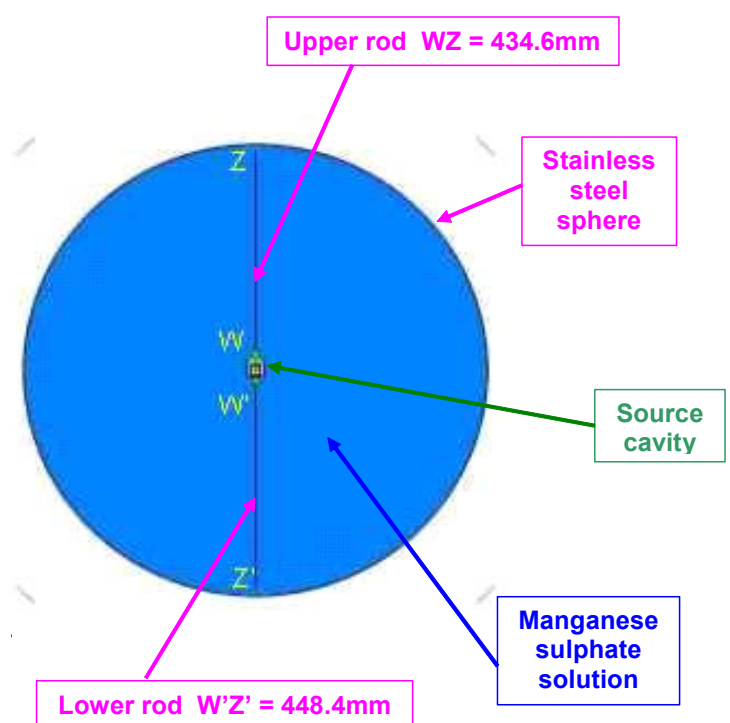


Figure 1. Manganese sulphate solution bath

Figure 2 shows an enlargement of the central cavity. The (AmBe) neutron source is installed in a cylindrical PMMA container. The symmetry axis of the source and holder is in coincidence with the vertical diameter of the spherical tank and the positioning of this source holder in the central part of the manganese sulphate

solution is achieved by a simple mechanical device represented by the upper and lower metallic rods. The dimensions of the source cavity are given in Appendix 1 and the PMMA composition in Appendix 2.

The geometrical centre of the radioactive material is positioned at the centre of the spherical tank, and the source characteristics (capsule and radioactive material), which are derived from manufacturer's data, can be found in Appendix 1. The neutron spectrum emitted by volume element is assumed to fit the (AmBe) energy distribution as recommended by the ISO 8529-1 Standard (2001) with an isotropic distribution (c.f. Appendix 3).

In a first approach, the Mn bath facility is located in an infinite vacuum. The influence of air and laboratory environment will be considered in a second stage.

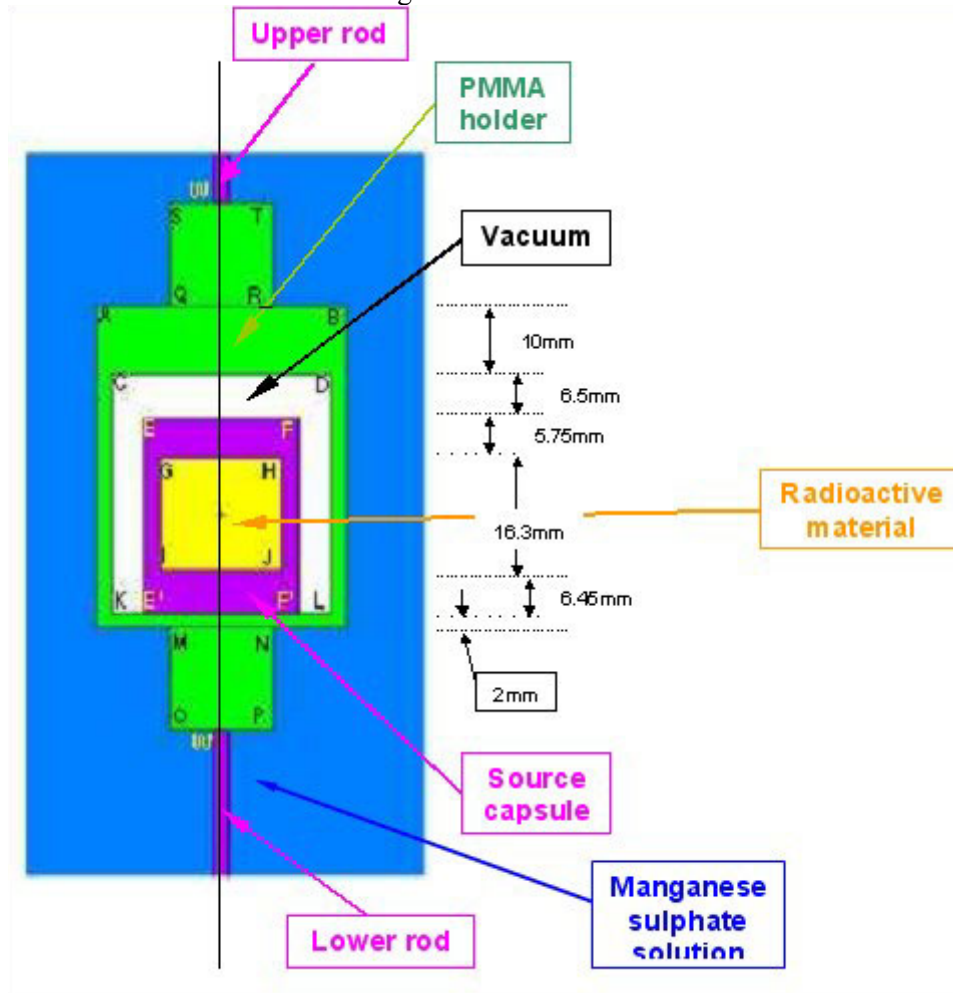


Figure 2. (AmBe) source and PMMA central cavity

Part 2, realistic model - Proposed tasks

The following tasks are proposed in which *all results should be normalised per neutron emitted from the source*, i.e. one neutron effectively leaving the exterior surface of the source capsule. This condition differs from usual simulations, which refer to 1 particle starting in the source.

From equation (3) above, it appears that the determination of the source strength (B) depends on several correction factors. Some of them can only be determined by calculations. Considering the various nuclear reactions involved in the set-up, the following tasks are proposed in this problem:

1. Evaluation of the self-absorption of neutrons in the source and derived spectral modifications. Please comment about these items.
2. Determination of the neutron fraction “recaptured” by the radioactive material and the source capsule after being emitted by the source. Please give a short description of the method that is applied to solve this question and justify the choice.

3. Determination of the neutron fraction captured in the cavity materials (PMMA holder and extensions, metallic rods)
4. Determination of the neutron fraction captured in the manganese sulphate solution.
5. Determination of the neutron fraction captured in the Mn of the bath solution [(n, γ) interactions]
6. Determination of the neutron fraction captured in S [(n, γ), (n,p), (n, α), total interactions]
7. Determination of the neutron fraction captured in O [(n, α) interactions]
8. Determination of the neutron fraction captured in H [(n, γ) interactions]
9. Investigation of the neutron leakage from the manganese bath facility. A concentric spherical surface (radius = 70 cm) will be considered for that purpose and the neutron contribution will be evaluated on that surface.
 - 9.1 Determination of the neutron fraction escaping the manganese bath facility
 - 9.2 Determination of the neutron fluence spectrum. Detailed energy binning of the neutron distributions and their graphical representation are given in Appendix 3.

Optional 1: Replace “vacuum” by “air” in the source cavity and outside the spherical tank and evaluate the consequences for some results, which may change.

Optional 2: The manganese bath set-up is installed in a laboratory. Estimate the influence of the concrete floor and walls on some calculated results (see walls dimensions and their positioning in Appendix 4).

Uncertainty analysis

The evaluation of uncertainties on calculated results may be derived from uncertainties assigned to the different elements of the modelled set-up.

Some of them can be straightforward dealt with by codes by applying the differential operator perturbation technique in the Monte Carlo method. As an example, in spite of limitations, the MCNP feature named “PERT card”, enables to treat different cases involving changes in cell materials, material compositions, densities, cross-sections, etc. For other cases, a specific and briefly described procedure should be employed. In addition to the stochastic uncertainties assigned to the numerical values provided by calculations, it is asked to establish the overall uncertainty attributed to the non-experimental terms (or correction factors) appearing in expression (1) of Section 2, by taking into account the following input data.

- a) Uncertainties on the density of the solution. The relative standard deviation on the density is 0.5 %.
- b) Uncertainty on the density of the (AmBe) radioactive material. The relative standard deviation on the density is assumed to be 20 %.
- c) Standard deviation of the position of the source centre with respect to the sphere centre: 10 mm
- d) Standard deviation of the sphere radius: 5 mm.
- e) Participants are free to use the interaction cross sections they consider as the ‘best’ ones. But, it is asked:
 - to give the bibliographic reference,
 - to clearly mention the uncertainties assigned to those basic data,
 - to evaluate the uncertainty on the results which are derived.

Experimental results and validation

When considering the set of measurements involved in the procedure for the determination of the neutron source strength through the manganese bath technique, the measured value of the neutron leakage component and the activity of the radionuclides created in the bath can be used to validate the calculated results.

The leakage can be estimated with a standard neutron source using a “de Pangher Long Counter” (PLC) to perform the measurement. This measurement is not straightforward and the experimentalist has to face difficulties inherent to the characteristics of the PLC, particularly the position of its effective centre. Nevertheless a comparison of both numerical values, with the associated uncertainties, should provide a

significant validation test of the computational model representing the manganese sulphate bath calibration facility.

The second experimental validation concerns the activity measurement of ^{56}Mn at saturation. This will be performed using a standard neutron source and a primary activity measurement technique, the 4π (Cerenkov)- γ coincidence counting. In addition, the activity evolution of ^{32}P (and if possible ^{35}S) with time will also be measured using liquid scintillation counting.

Characterisation of the PLC and measurements of the neutron leakage fluence as well as a budget of overall uncertainty involved in an international comparison exercise has been recently performed. Other validation measurements should be undertaken during the CONRAD-WP4 intercomparison exercise to crosscheck the current results.

Problem proposed by:

Jean-Louis Chartier , les Essarts-le-Roi, F and P. Cassette DRT-LNHB Saclay F

TO PRESERVE THE SCOPE OF THE COMPARISON ON THE EIGHT PROBLEMS, THE PARTICIPANTS ARE ASKED NOT TO PUBLISH THEIR RESULTS IN THE OPEN LITERATURE BEFORE THE FINAL WORKSHOP (AUTUMN 2007).

Correspondence:
Results should be returned to:
Jean-Louis Chartier
18 rue d'Yvette 78690 les Essarts-le-Roi, France
moloubis@yahoo.fr

Appendix 1

Geometry

(AmBe) source (see Figure 2)

- a) Capsule: material: stainless steel 316L
Cylindrical shell: outer diameter $EF = E'F' = 22.4$ mm
inner diameter $GH = IJ = 17.6$ mm
outer height $EE' = FF' = 28.5$ mm
inner height $GI = HJ = 16.3$ mm
upper wall thickness = 5.75 mm
lower wall thickness = 6.45 mm

- b) Radioactive material: mixture of AmO_2 and Be
Cylindrical shape: diameter $GH = IJ = 17.6$ mm
height $GI = HJ = 16.3$ mm

Note: the geometrical centres of the radioactive material and capsule do not coincide.

PMMA central cavity (see Figure 2)

PMMA holder:

- a) Cylindrical PMMA shell: outer diameter $AB = 36$ mm
inner diameter $CD = KL = 32$ mm
outer height (see Fig.2) = 47 mm
inner height $CK = DL = 35$ mm
upper wall thickness = 10 mm

lower wall thickness = 2 mm

b) Cylindrical upper and lower PMMA extensions: diameter MN = QR = 15 mm
height SQ = MO = 15 mm

Steel upper and lower rods (see Figure 1)

Stainless steel 316L, $\rho_{ss} = 7.90 \text{ g cm}^{-3}$
Cylindrical shape: diameter 2 mm
length upper rod: 434.6 mm
“ lower rod: 448.4 mm

Manganese bath sphere (see Figure 1)

Stainless steel 316L, $\rho_{ss} = 7.90 \text{ g cm}^{-3}$
Spherical steel shell: outer diameter = 1000 mm
inner diameter = 995 mm

Appendix 2

Material compositions

Table 1
Isotopic composition of natural sulphur

Isotope	Atomic fraction	Absolute uncertainty
^{32}S	0.9493	0.0031
^{33}S	0.0076	0.0002
^{34}S	0.0429	0.0028
^{36}S	0.0002	0.0001

Table 2
Composition in weight fraction of the manganese sulphate solution,
($\rho_{\text{sol}} = (1.288 \pm 0.006) \text{ g cm}^{-3}$)

Element	Weight fraction
Mn	$9.266 \cdot 10^{-2}$
S	$5.391 \cdot 10^{-2}$
O	$77.069 \cdot 10^{-2}$
H	$8.284 \cdot 10^{-2}$

Table 3
Composition in weight fraction of stainless steel 316L
($\rho_{ss} = 7.90 \text{ g cm}^{-3}$)

Element	Weight fraction
C	$2.6 \cdot 10^{-4}$
Mn	$1.4 \cdot 10^{-2}$
Si	$7.2 \cdot 10^{-3}$
P	$1.02 \cdot 10^{-2}$
Cr	$1.7 \cdot 10^{-1}$
Mo	$2.11 \cdot 10^{-2}$
Ni	$1.1 \cdot 10^{-1}$
Fe	$6.7 \cdot 10^{-1}$

S	$2.0 \cdot 10^{-4}$
---	---------------------

Table 4
Composition in atomic fraction of AmBe core of the source
($\rho_{\text{m}} = (1.12 \pm 0.22) \text{ g cm}^{-3}$)

Element	Atomic fraction
Am	0.00220
Be	0.99339
O	0.00441

Table 5
Composition of PMMA in weight fraction
($\rho_{\text{PMMA}} = (1.19 \pm 0.01) \text{ g cm}^{-3}$)

Element	Weight fraction
C	0.60
O	0.32
H	0.08

Table 6
Composition of air in weight fraction
($\rho_{\text{air}} = 1.20484 \cdot 10^{-3} \text{ g cm}^{-3}$)

Element	Weight fraction
C	0.000125
N	0.755267
O	0.231781
Ar	0.012827

Table 7
Composition of concrete in atomic fraction
($\rho_{\text{concrete}} = (2.3 \pm 0.2) \text{ g cm}^{-3}$)

Element	Atomic fraction
H	0.117
O	0.6082
Si	0.2748

Appendix 3

Information concerning the graphical representation of neutron spectra and the (AmBe) ISO 8529-1 neutron spectrum

Neutron fluence spectrum per lethargy unit

Histogram in log(abs)-lin(ord.) scales

Energy binning (upper bin boundaries):

1.0E-9	2.E-9	3.E-9	5.E-9	7.E-9
1.E-8	1.4E-8	2.E-8	3.E-8	4.E-8
5.E-8	6.E-8	7.E-8	8.E-8	9.E-8
1.4E-7	2.E-7	4.14E-7	1.E-6	1.E-5
5.E-5	1.E-4	2.E-4	4.E-4	7.E-4
1.E-3	3.E-3	6.E-3	1.E-2	2.E-2
2.2E-2	2.6E-2	3.E-2	4.E-2	6.E-2
8.E-2	0.11	0.33	0.54	0.75
0.97	1.18	1.40	1.61	1.82
2.04	2.25	2.47	2.68	2.90
3.11	3.32	3.54	3.75	3.97
4.18	4.39	4.61	4.82	5.04
5.25	5.47	5.68	5.89	6.11
6.32	6.54	6.75	6.96	7.18
7.39	7.61	7.82	8.03	8.25
8.46	8.68	8.89	9.11	9.32
9.53	9.75	9.96	10.18	10.39
10.60	10.82	11.03	12.0	13.0
14.0	15.0	16.0	17.0	20.0

ISO Standard 8529-1 (2001) (AmBe) neutron spectrum:

Energy binning (upper bin boundaries):

4.14E-7	0.11	0.33	0.54	0.75	0.97	1.18	1.40	1.61	1.82
2.04	2.25	2.47	2.68	2.90	3.11	3.32	3.54	3.75	3.97
4.18	4.39	4.61	4.82	5.04	5.25	5.47	5.68	5.89	6.11
6.32	6.54	6.75	6.96	7.18	7.39	7.61	7.82	8.03	8.25
8.46	8.68	8.89	9.11	9.32	9.53	9.75	9.96	10.18	10.39
10.60	10.82	11.03	11.09						

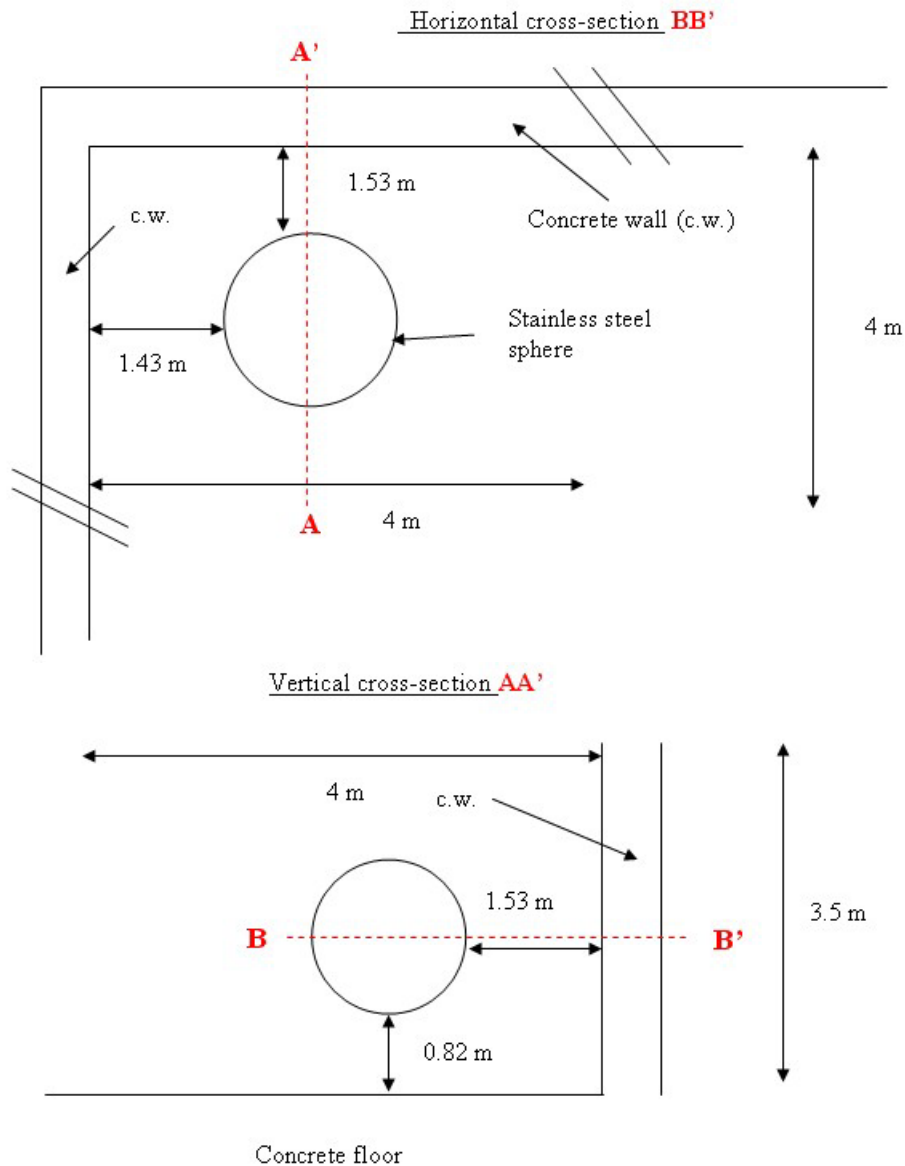
Probabilities:

0.0	1.44E-2	3.34E-2	3.13E-2	2.81E-2	2.50E-2				
	2.14E-2	1.98E-2	1.75E-2	1.92E-2	2.23E-2				
	2.15E-2	2.25E-2	2.28E-2	2.95E-2	3.56E-2				
	3.69E-2	3.46E-2	3.07E-2	3.00E-2	2.69E-2				
	2.86E-2	3.18E-2	3.07E-2	3.33E-2	3.04E-2				
	2.74E-2	2.33E-2	2.06E-2	1.82E-2	1.77E-2				
	2.04E-2	1.83E-2	1.63E-2	1.68E-2	1.68E-2				
	1.88E-2	1.84E-2	1.69E-2	1.44E-2	9.68E-3				
	6.52E-3	4.26E-3	3.67E-3	3.81E-3	5.06E-3				
	6.25E-3	5.52E-3	4.68E-3	3.70E-3	2.78E-3				
	1.51E-3	3.63E-4	0.0						

Appendix 4

Sphere environment (optional) (not to scale)

The stainless steel sphere containing the manganese sulfate bath is placed near two 50 cm thick perpendicular concrete walls and 0.82 meter above a concrete floor (1 meter thick)
The distances between the sphere and the 2 walls are given in the sketch below
The height of walls above the floor is 3.5 meters



P6- IRON SPHERE EXPERIMENTS

Problem

Calculate the neutron spectra leaking from five iron shells with ~14 MeV neutron source in the centre. The spheres have radii from 4.5 to 30.0 cm and wall thicknesses from 2.5 to 28.0 cm. Neutron leakage spectra measured by the time-of-flight technique in the 0.05-15 MeV energy range are available.

Source Specifications and Experimental Configuration

The source was a T(d,n) ~14 MeV neutron source located at the centre of the iron spheres. Pulsed beam of deuterons with kinetic energy of 280 keV was injected to a solid Titanium-Tritium target. The ion pulse width was 2.5 ns. The Ti-T target was a thin layer deposited on 1 mm thick copper (Fig. 3). Since the TiT layer is very thin its influence on the neutron attenuation may be neglected. The deuteron beam spot width was ~6 mm, therefore the neutron source should be taken as distributed on the disc of 6 mm in diameter, placed at $x=0$ (Fig. 3). The mean energy and yield of the neutron source peak were slightly angle dependent, as shown in Table 5. The data are available from CONRAD web page (<http://www.nea.fr/download/quados/Conrad/conrad.html>) in the file Fe_shells-tables.xls (Neutron source) and on request from the author (see correspondence).

Five spherical shells of pure iron were available for the experiment. They are shown in Figure 2. Their dimensions are given in Figure 2 and Table 6. The material densities and compositions are given in Tables 1 and 2.

Description of the Beam tube (see Figs. 1 and 3):

Beam tube made of Al and wall thickness 0.5 mm had a form of cone extending from 32 cm from the shell to the centre of the shell. T-Ti layer was deposited on a copper target with a radius of 0.5 cm and thickness of 0.1 cm (Figure 3). The Ti-T target was placed at the centre of the iron spheres. The densities and compositions of the beam tube materials are given in Table 3.

Measurement System and Uncertainties

The detector used was a fast scintillator detector located at an angle of 8 deg. relative to beam trajectory extension and at a flight path of 6.8 m. The detector itself consisted of a cylindrical paraterphenyl crystal of 5 cm diameter and 5 cm height. It was coupled to a FEU-143 photomultiplier. The detector has a time resolution of 3 ns and background γ -ray suppression by the pulse-shape discrimination technique.

The time-of-flight measurement was made in the usual inverse method, i.e. using the detector signal as a start signal and the delayed deuteron pick-up pulse as a stop signal. In this way only the useful neutron bursts, i.e. those producing a signal in the detector are used, so avoiding dead time losses.

The experimental spectra were corrected for the background effects. To measure the background neutron spectra, a 1 m long by 18 - 26 cm diameter iron shadow bar and a 30 cm long borated polyethylene cylinder were placed between the detector and the sphere (Figure 1).

The neutron detector efficiency was experimentally determined by measuring the spectrum of neutrons from the spontaneous fission of ^{252}Cf , which is known in the range 0.1-10 MeV with 3% accuracy. For this purpose a californium fission chamber (about $5 \cdot 10^5$ disintegrations per second) was periodically used during the measurements. The efficiency at 14 MeV neutron energy, more affected by the finite time resolution and collimator scattering effects than lower energy neutrons, was measured using the bare T(d,n) neutron source with the associated α -particles technique. The measured spectrum for the bare detector can be used to deduce the energy resolution of the detector around 14 MeV. The spectrum is given in Table 7 and in the file Fe_shells-tables.xls (Spectrometer response function) (see <http://www.nea.fr/download/quados/Conrad/conrad.html>).

The estimated uncertainties of the experimental data and their main components are listed in Table 4.

Neutron spectra measurements

The measured time-of-flight (TOF) spectra were corrected for the background effects and converted to the energy spectrum. The TOF spectra were transformed to energy spectra according with:

$$E = m_0 c^2 \left(\frac{1}{\sqrt{1 - (L/c \cdot t)^2}} - 1 \right) \quad (1)$$

where: m_0 - neutron mass ($m_0 c^2 = 939.56563$ MeV),
 c - speed of light in vacuum (= 0.299792458 m/ns),
 L - flight path (6.8 m),
 t - time of flight in ns

In the case of neutron velocity $v = L/t \ll c$, this relation transforms to the classical one (convenient only for simple assessments):

$$E [MeV] \approx \frac{m_0}{2} (L[m]/t[ns])^2 \quad (2)$$

The TOF spectrum $dN(t)/dt$ can be transformed to the energy spectrum $dN(E)/dE$ according to:

$$\frac{dN(E(t))}{dE} = \frac{dN(t)}{dt} \cdot \left(\frac{\partial E(t)}{\partial t} \right)^{-1} \quad (3)$$

where the derivative dE/dt is obtained from (1) as:

$$\frac{\partial E(t)}{\partial t} = \frac{m_0}{t} \frac{v^2}{(1 - (v/c)^2)^{3/2}} \quad (4)$$

$v = L/t$ - neutron velocity

The leakage spectrum, $dL(E)/dE$, representing the differential fluence of leakage neutrons, integrated over the full sphere (4π sr) and normalised to 1 source neutron, was then calculated from the following expression:

$$\frac{dL(E)}{dE} = \frac{dN(E)}{dE} \cdot \frac{4\pi}{\varepsilon(E) \cdot \Delta\Omega \cdot N_n} \quad (5)$$

where:

$N(E)$ = neutron energy spectrum, converted from measured TOF spectra,

$\varepsilon(E)$ = neutron detection efficiency,

$\Delta\Omega$ = detector solid angle (= $\pi r^2 / L^2$, where r is the detector radius and L the distance from the sphere to the detector centre),

N_n = number of source neutrons.

The neutron leakage spectra together with the associated uncertainties are tabulated in the file Fe_shells-tables.xls (Neutron spectra) available from our web page <http://www.nea.fr/download/quados/Conrad/conrad.html>.

Scope of the exercise

The neutron spectra are to be calculated as leakage spectrum defined in Eq. (5), i.e. in terms of neutrons per MeV and per source neutron, for the iron shells with the following radii and wall thicknesses:

1. $r=4.5$ cm, wall thickness = 2.5 cm,
2. $r=12.0$ cm, wall thickness = 7.5 cm,
3. $r=12.0$ cm, wall thickness =10.0 cm,
4. $r=20.0$ cm, wall thickness =18.1 cm,
5. $r=30.0$ cm, wall thickness =28.0 cm.

A subset of the above, including at least shells 1 and 5, can be considered.

For an adequate comparison of measurements and analytical calculation near the 14 MeV peak, the convolution with the spectrometer response function, describing the energy resolution of the spectrometer, is necessary. Note that neutrons with energies lower than 14 MeV may also require similar corrections for finite detector time resolution, using appropriately transformed response function. For the purpose of the exercise the solutions applying this correction only to 14 MeV peak will be accepted.

Due to its small size as compared to the distance from the shell the detector can be modelled as point detector.

For shells 4 and 5: Note that the spectra can be obtained in two ways:

- neutron energy spectra calculation (time independent)
- neutron TOF spectra calculation (time dependent). Neutron energy spectra for the comparison with the tabulated measured spectra are obtained using the Equations (1) to (5).

Compare the neutron spectra in the ~0.1-15 MeV energy range obtained using the above two approaches and discuss the eventual differences you observe (shells 4 and 5).

Estimate the uncertainties in the calculated neutron spectra, caused by the method and nuclear data uncertainties (e.g. material density, cross sections).

Verify if the agreement between the calculation and experiment is within the overall (computational and measurement) uncertainties.

Table 1: Iron spheres dimensions, material and nuclear density.

<i>Sphere No.</i>	<i>Material density (g/cm³)</i>	<i>Iron (mass %)</i>	<i>Fe atomic number density (10²² Fe at./cm³)</i>
1	7.793 ± 0.004	99.8	8.385
2	7.679 ± 0.002	99.1	8.206
3	7.684 ± 0.002	99.1	8.210
4	7.800 ± 0.078	99.0	8.329
5	7.800 ± 0.078	99.0	8.329

Table 2: Impurities (mass %) of the iron spheres

<i>Element</i>	<i>Sphere 1</i>	<i>Sphere 2</i>	<i>Sphere 3</i>	<i>Sphere 4</i>	<i>Sphere 5</i>
Carbon	0.22	0.15	0.15	0.20	0.20
Silicon				0.27	0.27
Chromium		0.30	0.30		
Manganese		0.45	0.45	0.50	0.50

Table 3: Composition (w%) and densities of Beam tube materials

<i>Element</i>	<i>Copper</i>	<i>Aluminium</i>	<i>Stainless Steel</i>
Fe			0.6993
Ni			0.09
Cr			0.18
Mn			0.02
Si			0.01
C			0.0007
Cu	1.0		
Al		1.0	
Density (g/cm³)	8.96	2.7	7.9

Table 4: Measurement uncertainties

<i>Component</i>	<i>Value</i>	<i>Energy Dependence</i>
Statistics	1 to 50%	Yes
Stability of equipment	3 to 5%	Yes
Cf-252 fission spectrum	1 to 3%	Yes
Pu-238 alfa-intensity	2%	No
Cf-chamber scattering	1%	No
TOF-to-energy conversion	2%	No
Total	5 to 50%	Yes

Table 5: Neutron source energy and angular distribution.

<i>Angle cos(θ)</i>	<i>Relative neutron yields</i>	<i>Neutron Energy (MeV)</i>	<i>Angle cos(θ)</i>	<i>Relative neutron yields</i>	<i>Neutron Energy (MeV)</i>
-1	0.874	13.36	0.0872	0.941	14.165
-0.9962	0.874	13.365	0.1737	0.946	14.23
-0.9848	0.875	13.37	0.2588	0.952	14.32
-0.9659	0.876	13.385	0.342	0.957	14.4
-0.9397	0.877	13.4	0.4226	0.962	14.44
-0.9063	0.879	13.425	0.5	0.967	14.48
-0.866	0.882	13.45	0.5736	0.972	14.54
-0.8192	0.884	13.49	0.6428	0.976	14.6
-0.766	0.888	13.53	0.7071	0.981	14.65
-0.7071	0.891	13.58	0.766	0.985	14.7
-0.6428	0.895	13.62	0.8192	0.988	14.74
-0.5736	0.899	13.67	0.866	0.991	14.78
-0.5	0.904	13.71	0.9063	0.994	14.81
-0.4226	0.909	13.8	0.9397	0.996	14.84
-0.342	0.914	13.88	0.9659	0.998	14.86
-0.2588	0.919	13.92	0.9848	0.999	14.88
-0.1737	0.924	13.97	0.9962	1	14.885
-0.0872	0.93	14.04	1	1	14.89
0	0.935	14.1			

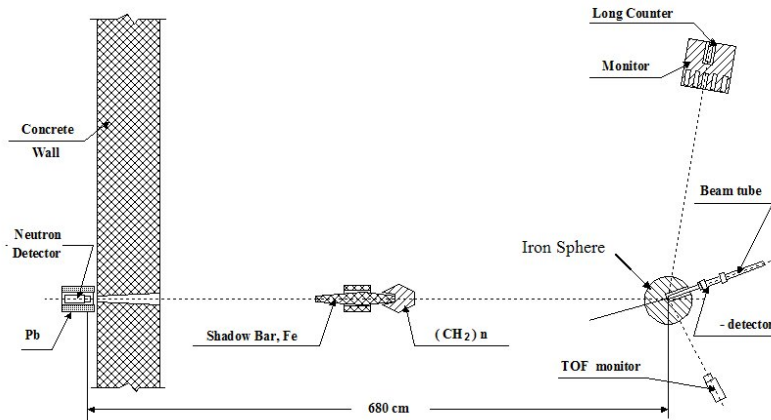


Fig. 1. Lay-out of experiment for measuring the neutron leakage spectra from iron spheres.

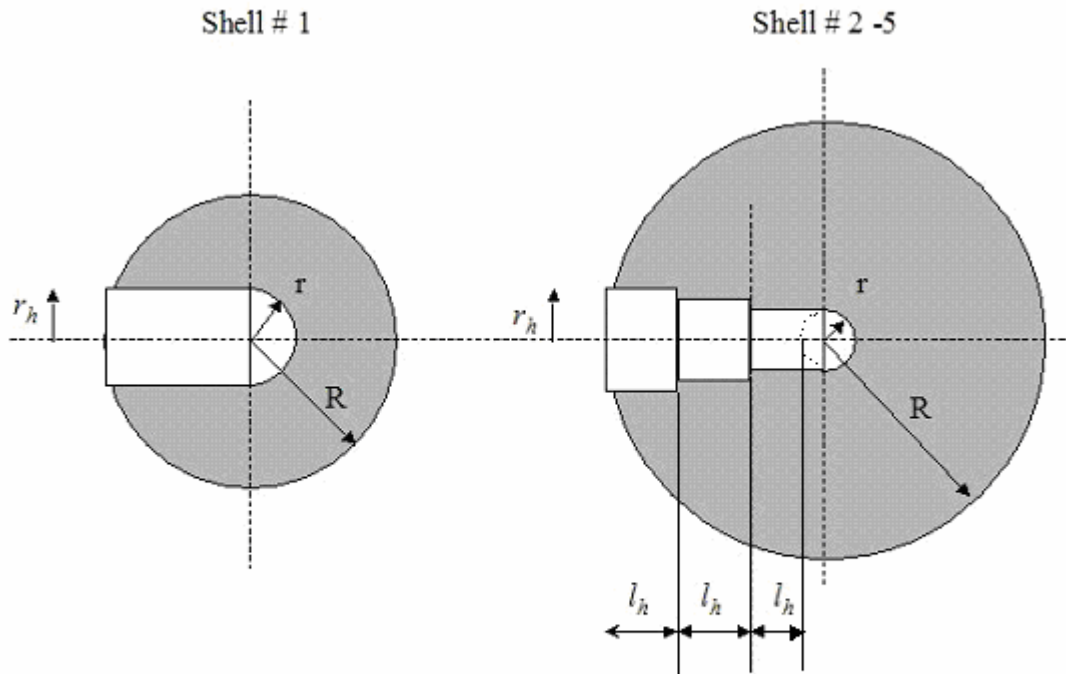


Fig. 2. Configuration of the iron shells #1 (left) and shells #2 - #5 (right).
Sizes are listed in the Table below.

Table 6: Iron spheres dimensions, material and nuclear density (see Fig. 2 for details and definitions). The values for the sets $r_h(l_h)$, up to three depending on the sphere, are given from left to right as in the above Figure 2.

Sphere No.	Outer Radius - R (cm)	Hole Radius - r (cm)	Thickness $R - r$ (cm)	Hole configuration $r_h(l_h)$ (cm)	S_h / V (%)
1	4.5	2.0	2.5	2.0(2.5)	10.6
2	12.0	4.5	7.5	3.2(4), 3.0(3.5)	3.3
3	12.0	2.0	10.0	3.2(4), 3.0(3.5), 2.0(2.5)	3.7
4	20.0	1.9	18.1	2.5(10.3), 1.9(7.8)	0.9
5	30.0	2.0	28.0	4(7), 2.5(7.8), 2.0(13.2)	0.6

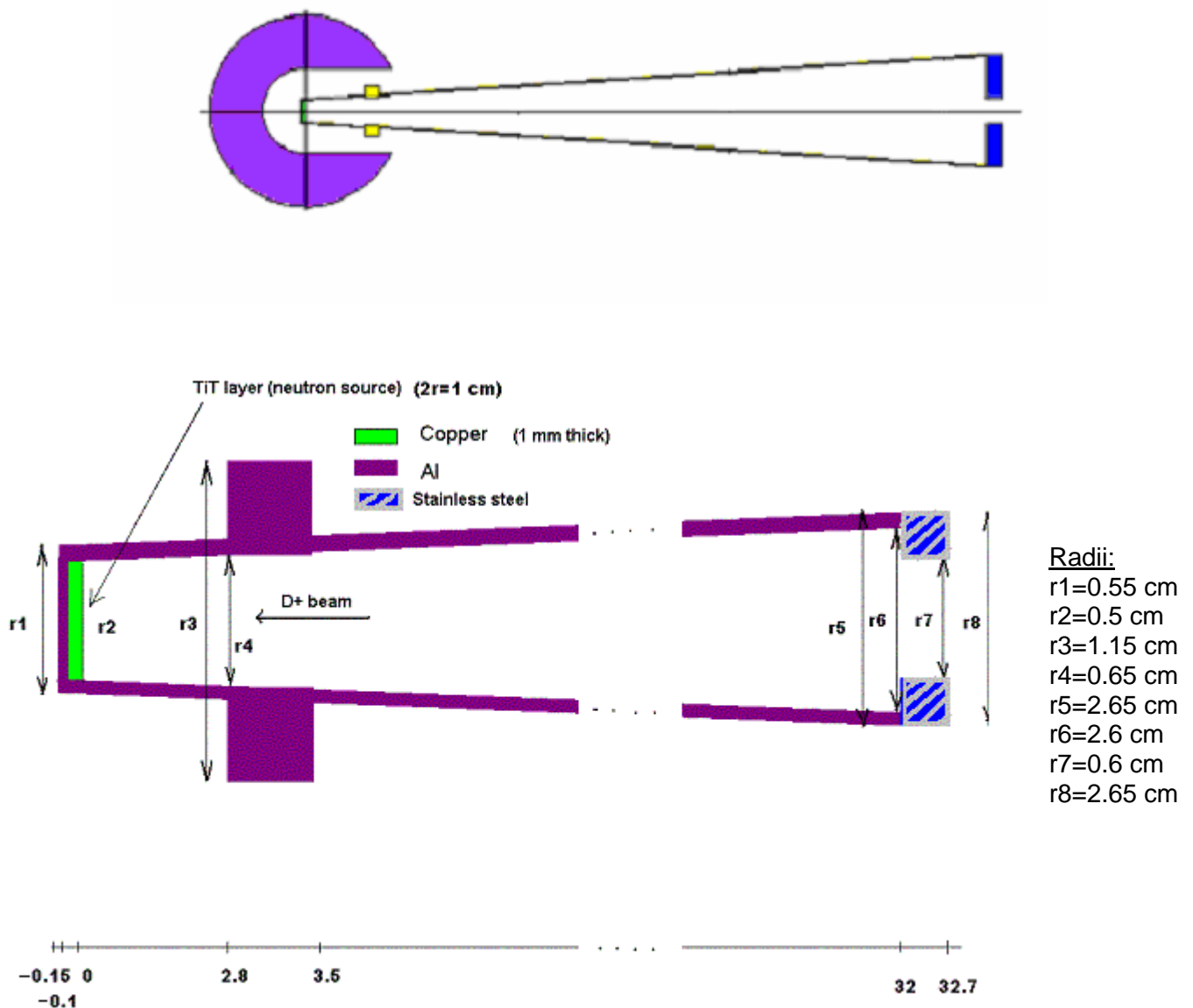


Fig. 3. Scheme of the beam tube. Above is the Iron shell 1 with the beam tube (realistic proportions) and figure below shows details of the beam tube (schematic, not to scale!). Beam tube was made of aluminium with wall thickness of 0.5 mm. It was in a form of cone extending from a distance of 32 cm from the shell to the centre of the shell. The Ti-T target deposited on a 1 mm thick copper layer was placed at the sphere centre, located at $x=0$ cm. Two screws, the first made of aluminium and the second of stainless steel, can be modelled as cylinders. See Figure 1 for the actual position of the beam tube in the experimental setup.

Table 7: Spectrometer response function (neutron spectrum measured without iron shells).

Secondary Neutron Energy (MeV)	Spectrum Response Function (n/MeV/source n)	Total relative Uncertainty	Secondary Neutron Energy (MeV)	Spectrum Response Function (n/MeV/source n)	Total relative Uncertainty
2.934	2.65E-04	122.90%	7.144	1.74E-03	17.12%
2.982	1.46E-04	220.70%	7.253	1.79E-03	15.35%
3.03	4.70E-05	739.90%	7.364	1.76E-03	15.21%
3.08	3.24E-04	93.26%	7.439	1.66E-03	15.10%
3.131	1.03E-04	268.10%	7.555	1.81E-03	13.73%
3.184	1.11E-04	413.20%	7.673	1.58E-03	14.60%
3.227	6.62E-04	71.91%	7.753	1.39E-03	16.52%
3.282	3.94E-04	84.73%	7.835	1.96E-03	12.30%
3.338	4.79E-04	97.01%	7.96	1.80E-03	13.84%
3.384	1.86E-04	428.20%	8.132	2.00E-03	13.06%
3.431	9.59E-04	47.94%	8.309	1.99E-03	12.76%
3.479	8.36E-04	53.96%	8.491	2.13E-03	11.84%
3.528	5.99E-04	74.22%	8.68	2.52E-03	10.18%
3.578	3.74E-04	123.90%	8.876	2.66E-03	9.36%
3.63	8.68E-04	49.43%	9.078	2.66E-03	9.35%
3.682	6.85E-04	59.66%	9.287	2.67E-03	8.90%
3.735	4.06E-04	98.25%	9.503	3.08E-03	7.70%
3.79	2.35E-04	202.00%	9.728	3.27E-03	7.26%
3.832	9.46E-04	44.80%	9.901	3.61E-03	6.63%
3.874	8.69E-04	47.87%	10.08	3.68E-03	6.43%
3.932	8.24E-04	49.30%	10.32	4.08E-03	5.81%
3.976	7.83E-04	53.53%	10.51	4.15E-03	5.68%
4.051	7.56E-04	72.28%	10.71	4.51E-03	5.18%
4.16	8.29E-04	37.61%	10.91	5.19E-03	4.59%
4.257	8.33E-04	34.28%	11.12	5.75E-03	4.22%
4.358	9.57E-04	29.41%	11.33	6.19E-03	3.97%
4.462	1.00E-03	23.83%	11.47	6.77E-03	3.67%
4.551	5.58E-04	54.67%	11.7	7.24E-03	3.42%
4.643	6.21E-04	37.03%	11.92	8.51E-03	3.09%
4.758	8.80E-04	29.52%	12.08	9.36E-03	2.86%
4.856	1.04E-03	37.07%	12.32	1.00E-02	2.71%
4.958	1.09E-03	49.48%	12.57	1.15E-02	2.44%
5.063	1.36E-03	27.23%	12.74	1.36E-02	2.21%
5.15	1.14E-03	30.94%	12.91	1.55E-02	2.04%
5.238	1.07E-03	64.90%	13.09	1.86E-02	1.83%
5.352	1.11E-03	21.47%	13.27	2.37E-02	1.61%
5.47	1.23E-03	31.24%	13.45	3.26E-02	1.36%
5.567	1.07E-03	31.16%	13.64	4.91E-02	1.11%
5.667	1.09E-03	31.07%	13.83	8.66E-02	0.87%
5.77	1.15E-03	27.76%	14.03	1.68E-01	0.68%
5.875	1.08E-03	31.69%	14.23	3.16E-01	0.58%
5.956	1.50E-03	21.06%	14.43	5.33E-01	0.52%
6.038	1.14E-03	36.92%	14.64	7.46E-01	0.50%
6.151	1.67E-03	18.58%	14.86	8.28E-01	0.49%
6.267	1.20E-03	31.75%	15.08	7.24E-01	0.50%
6.356	9.85E-04	27.73%	15.3	4.84E-01	0.53%
6.447	1.40E-03	21.29%	15.53	2.36E-01	0.60%
6.572	1.32E-03	22.56%	15.76	7.85E-02	0.83%
6.668	1.37E-03	21.44%	16	1.65E-02	1.60%
6.766	1.55E-03	19.95%	16.25	2.53E-03	4.50%
6.866	2.01E-03	15.47%	16.5	6.90E-04	11.27%
6.968	1.78E-03	16.93%	16.75	4.61E-04	15.66%
7.073	2.06E-03	14.50%	17.01	4.48E-04	15.18%

Tables 5 and 7 as well as the measured spectra are available in xls format (file **Fe_shells-tables.xls**) from the web page <http://www.nea.fr/download/quados/Conrad/conrad.html> and/or from the author (see below).

Problem proposed by:

I. Kodeli, IAEA representative at OECD-NEA Data, France (ivo.kodeli@oecd.org)

S.P. Simakov, Fz Karlsruhe, Germany (simakov@irs.fzk.de)

TO PRESERVE THE SCOPE OF THE COMPARISON ON THE EIGHT PROBLEMS, THE PARTICIPANTS ARE ASKED NOT TO PUBLISH THEIR RESULTS IN THE OPEN LITERATURE BEFORE THE FINAL WORKSHOP (AUTUMN 2007).

Correspondence:
Results should be returned to:
Ivo Kodeli
OECD-NEA Data Bank
12 Bd des Isles, 92 130 Issy Les Moulineaux
France ivo.kodeli@oecd.org

P7 - ENERGY RESPONSE CHARACTERISTICS OF A RADFET RADIATION DETECTOR

Introduction

The Metal-Oxide Semiconductor Field-Effect-Transistor (MOSFET) is frequently used as a sensor of ionizing radiation; when used in this way, the device is often called a RadFET. The radiation sensitivity of a RadFET is deliberately made to be as high as possible by manipulating the production process so that the device has a thick oxide-layer (typically about 400 nm). In comparison, a conventional 'radiation-hard' MOSFET will have an oxide layer that is a few nanometers thick. RadFET dosimeters have recently found numerous applications in nuclear-medicine, diagnostic-radiology, radiotherapy quality-assurance and in the nuclear and space industries. The key element in the operation of a RadFET is the MOS capacitor, formed from the Gate and its metallic contact; the oxide layer beneath the Gate and the silicon substrate. When a RadFET is exposed to ionizing radiation, mobile holes and electrons are produced in both the insulating oxide-layer and the Si-substrate. The mobile holes are trapped both in the bulk substrate and at the Si – SiO₂ interface and lead to a 'permanent' shift in the voltage required to switch the device on (the threshold-voltage); the energy deposited in the oxide layer can be directly related to the change in threshold voltage and thus the RadFET can be used as a dosimeter.

This problem is focused on calculating the energy response of a p-type RadFET to low-energy photons and on understanding the influence of uncertainties in the composition and geometry of the device in calculating the energy response function.

The complete structure of the device is rather complicated but since the primary element, in terms of radiation effect, is the MOS-capacitor, we are able to reduce the geometry to a simple stack of appropriate materials (Figure 3). Further, under the majority of conditions, the threshold-voltage shift is directly proportional to the energy deposited in the oxide-layer and thence to the absorbed dose, so we can effectively calculate the response of the dosimeter by correctly calculating the deposited energy in the oxide-layer.

Problem geometry

Figure 1 shows the overall geometry of a RadFET device and Figure 2 shows a stylized isometric sketch of the same device and defines the co-ordinate system. The MOS capacitor portion of the RadFET can be approximated with a stack of parallelepiped layers, as shown in Figure 3 (note, for brevity, not all of the regions shown in Figure 3 have been reproduced in Figure 1).

Figure 3 represents the simplified geometry to be modelled in this problem; it is a detail of the MOS capacitor Gate structure – the x-axis points from region 1 to region 11 and the y-axis increases left to right (i.e. the co-ordinate system is consistent with figure 2). In determining the energy deposition in the oxide-layer (region 5), it may be necessary to include some material that is in close proximity to the capacitor (such as the field oxide and Al contact) so as to take effect of energy deposited in the oxide-layer from charge generated laterally to that region – refer to Figures 1 and 2. The extent of the geometry simulated in the regions in proximity to the Gate oxide is up to the participant but you should justify and fully report your method (see problem 2 part V). Figure 4 shows the irradiation geometry: a plane parallel monoenergetic photon source is incident on the RadFET in the direction pointing from region 1 to region 11. The RadFET / source combination is situated in vacuo.

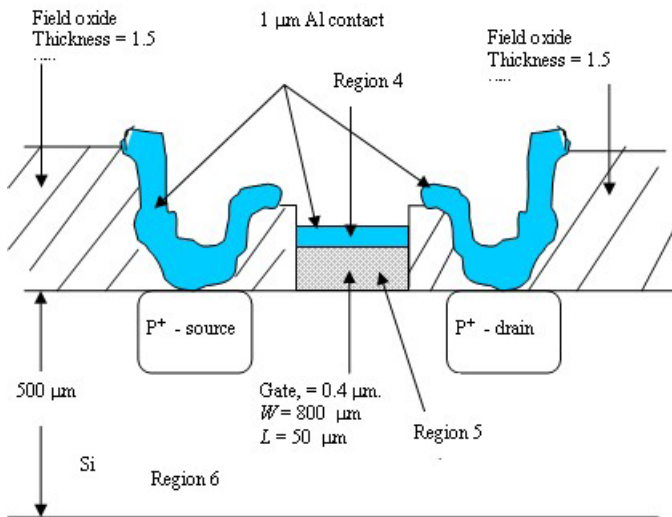


Figure 1: RadFET structure. The MOS capacitor is the parallelepiped region above and below the gate. See figure 2 for the definition of the oxide width (W) and length (L). The full MOS capacitor structure is shown in Figure 3

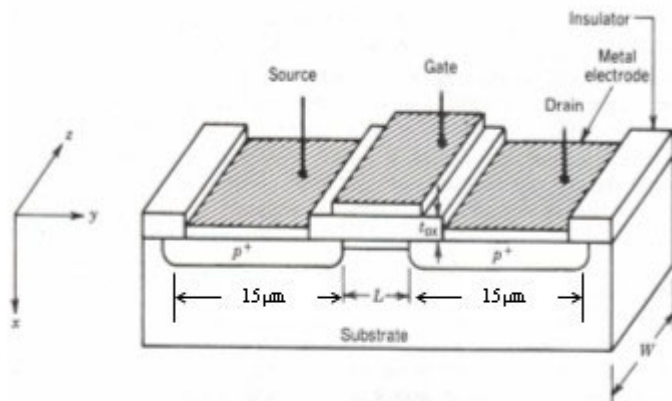


Figure 2: Isometric sketch of RadFET chip, indicating the meaning of W and L and the relative positions of each component in three dimensions. The oxide thickness is indicated as t_{ox} and W and L are identified.

Problem 1

In the first part of the problem you are asked to compute the energy response function of the RadFET and investigate the effect of the kovar cap – region 1 in figure 3. Calculate the energy deposition in region 5 over the energy range 12 keV to 2 MeV for sources of photons; your results should be normalised to unit air kerma incident on the RadFET and presented relative to the result for 1.1 MeV (approximately ^{60}Co energy). Present your results as a continuous response function. Calculate the energy response function for the

Region 1: 250 μm lid – 29%Ni, 17%Co, 54%Fe: Lid density = 8.4 g/cm^3
Region 2: 250 μm vacuum
Region 3: 0.2 μm thick passivation – Si_3N_4 : density = 3.4 g/cm^3
Region 4: 1 μm thick aluminium contact: density = 2.7 g/cm^3
Region 5: 0.4 μm thick gate oxide – SiO_2 : density = 2.27 g/cm^3
Region 6: 500 μm thick silicon substrate - Si: density = 2.3 g/cm^3
Region 7: 250 μm adhesive - 80% Ag, 20% SiO_2 : densities Ag=10.5, SiO_2 = 2.3 g/cm^3
Region 8: 1.5 μm Au attached pad A: density = 19.3 g/cm^3
Region 9: 2 μm Ni attach pad B: density = 8.9 g/cm^3
Region 10: 0.2 mm attach pad C - 90% W, 10% Cu : material density = 17 g/cm^3
Region 11: 1000 μm Al_2O_3 , base : density = 3.6 g/cm^3

Figure 3: The MOS capacitor region to be modelled

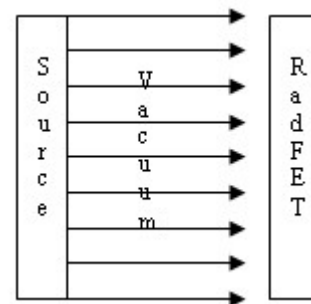


Figure 4: Irradiation geometry – plane parallel source in direction of regions 1 to 11 (+ ve x direction – figure 2).

following situations: 1) the device consisting of regions 1 through 11 – call this “capped device” and 2) the device with no cap – i.e. omit regions 1 and 2 – thus simulate only regions 3 to 11 – call this the “uncapped device”. In both cases, you should consider the photon energies: 20 keV, 35 keV, 48 keV, 65 keV, 100 keV, 118 keV and 208 keV and 1.1 MeV as a minimum data set. You should seek to clearly identify the energy at which the response maxima occur. You should take care to ensure that the simulation and energy deposition algorithms of the code you are using are not violated in the small volumes of the geometry considered.

Problem 2

In this problem you should investigate the sensitivity of your calculations to uncertainties in the composition and geometry of the device.

You should evaluate the uncertainty in energy deposition in the oxide layer for a plane parallel monoenergetic source.

You should consider an energy range about the photon energy identified in Problem 1 at which the response of the device is a maximum (for both cases – “capped device” and “uncapped device”).

Calculate the energy deposition in region 5:

a) for the “capped device”

- i) the effect of random uncertainties (up to 20%) in the thickness of region 1
- ii) the effect of random uncertainties (up to 20%) in the proportion of Ni in region 1

b) for the “uncapped device”

- iii) the effect of random uncertainties (up to 20%) in the proportion of Ag in region 7
- iv) the effect of a systematic under-estimate of 300 % in the thickness of region 8 (ie you should consider the effect of increasing the thickness of region 8 by 300 %).
- v) Determine the sensitivity of your solutions to the extent of the model in the y- and z-directions - in other words you are here asked to justify your model geometry.

TO PRESERVE THE SCOPE OF THE COMPARISON ON THE EIGHT PROBLEMS, THE PARTICIPANTS ARE ASKED NOT TO PUBLISH THEIR RESULTS IN THE OPEN LITERATURE BEFORE THE FINAL WORKSHOP (AUTUMN 2007).

Correspondence:

Results should be returned to:
Dr Robert A Price
City University
School of Allied Health Science
Northampton Square
London
r.price@city.ac.uk

P8 - RECOIL-PROTON TELESCOPE DETECTOR: SENSITIVITY AND UNCERTAINTY ANALYSIS

Introduction

This problem supplements the problem P1 introduced by S. Agosteo. Consider the same detector and the same neutron energies, given in Table 1 below.

Figure 1 shows the cross sectional view of a measurement for calibrating the recoil-proton telescope detector, *it is not to scale!* Figure 2 shows a so-called ΔE_p versus E_p plot, where ΔE_p is the energy of a proton deposited in the ΔE -layer and E_p is the sum of the proton energies deposited in the ΔE -layer and E -layer, i.e. the energy of a detected proton when leaving the Ti-dead-layer. Assume an ideal electronics and do not assume any dead times for the detector.

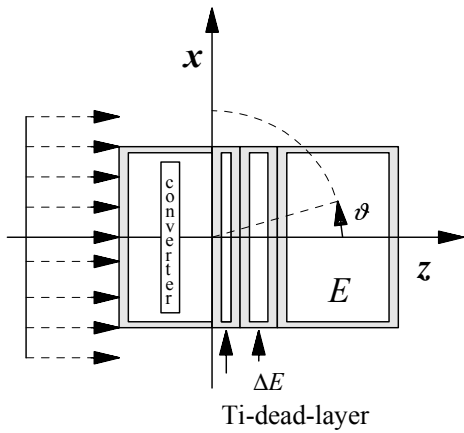


Figure 1. Cross sectional view of the recoil-proton telescope detector, *not to scale!* There are slight differences to the problem by Agosteo.

The dashed arrows on the left visualise the incident neutrons.

The $z=0$ plane coincides with the boundary between polyethylene converter and titanium dead layer. All interfaces coincide with x - y -planes.

The grey zones visualise uncertainties associated with geometrical specifications, i.e. width, height and thickness of the detector components.

The angle ϑ is referred to in the main text as tilting angle. Instead of tilting the detector one may change the direction of the source neutrons.

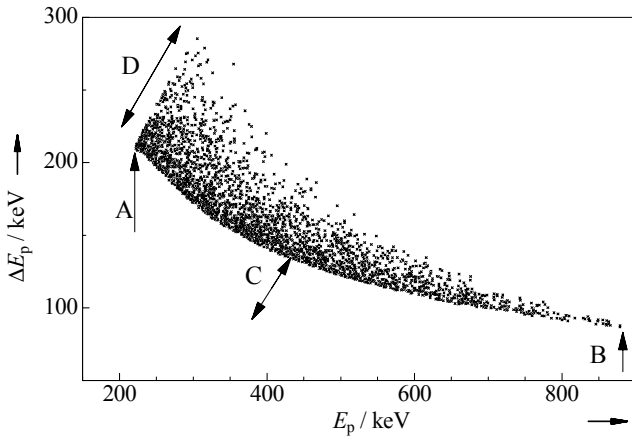


Figure 2. Proton energy ΔE_p deposited in the thin Si-layer as a function of the total proton energy E_p as deposited in the thin and the thick Si-layer. The data shown result from 1 MeV neutrons, normally incident on the polyethylene converter, i.e. the tilting angle $\vartheta=0^\circ$, see Figure 1. Only protons from first collisions produced via H(n,p) are shown. The labelled arrows indicate characteristic features, see task 3.

The proton field resulting from H(n,p) reactions in the polyethylene converter can be denoted by

$$\Phi_{E_p, r_p, \Omega_p}(E_p, \mathbf{r}_p, \boldsymbol{\Omega}_p) \equiv f_{\text{conv}}(E_p, x_p, y_p, z_p, c_{p,x}, c_{p,y}, c_{p,z}). \quad (1)$$

where the subscript “conv” indicates “generated in the converter” and E_p is the proton energy, x_p , y_p and z_p indicate the reaction site and $c_{p,x}$, $c_{p,y}$, and $c_{p,z}$ are the cosines of the direction of flight. Neglect multiple neutron scattering for the first two tasks.

First question

The *first task* is to generate the protons in the converter and to propagate them through the dead-layer, the ΔE -layer and to the E -layer and to compute the resulting proton fields f_{dead} , $f_{\Delta E}$ and f_E ; where the subscripts indicate the left boundaries of the indicated layers, see Figure 1. The marginal distributions $f_{\text{dead}}(E_p)$, $f_{\Delta E}(E_p)$ and $f_E(E_p)$ should be represented in tabular form and as plots with a bin width of 1 keV. Marginal means here “integrated over all direction and positions on the specified z-plane”. The results should be normalised to unit incident neutron fluence, i.e. 1 cm^{-2} . Furthermore a table with the mean proton energies and their variances at all interfaces should be compiled and Figure 2 above should be reproduced for the three mean neutron energies (bold print in the table). The **measurand is the response $R_{\text{PRT}}(E_n)$** of the detector, i.e. the number of protons triggering both, the ΔE -stage and the E -stage per unit neutron fluence. The unit of R_{PRT} is cm^2 .

Second question

The *second task* is to study the influence of the variation of the geometric data, the incident neutron energy and of tilting the detector *and* to propagate the uncertainties associated with the values of these input quantities via a *linear model*. Consider rectangular distributions for the examined input quantities and assume the following values:

- width and height: $(1000 \pm 20) \mu\text{m}$ for all layers,
- thickness: dead layer: $(0.24 \pm 0.02) \mu\text{m}$ and ΔE -layer $[(1.9 \pm 0.2) \mu\text{m}$,
- neutron energy: $(680 \pm 30) \text{ keV}$, $(996 \pm 40) \text{ keV}$ and $(1306 \pm 50) \text{ keV}$, see Table,
- tilting angle: $(0 \pm 5) \text{ degree}$,
- densities: $\rho(\text{CH}_2)=0.95 \text{ gcm}^{-3}$, $\rho(\text{Ti})=4.50 \text{ gcm}^{-3}$ and $\rho(\text{Si})=2.33 \text{ gcm}^{-3}$;

assume relative uncertainties of 1%.

Third question

The *third task* is to discuss and explain the characteristic features of the so-called ΔE_p versus E_p plot, as indicated by the labelled arrows in Figure 2, and to quantify the influence of variations in geometric specifications and incident neutron energy. In addition, the influence of multiple scattering and any other sources of uncertainty, e.g. range and straggling, should be discussed here, too. Finally, compare the uncertainty obtained in task 2 with that obtained by varying all input quantities simultaneously by means of Monte Carlo integration.

The basic intent of this problem is to prompt the participant to derive the answers without general purpose Monte Carlo codes but rather using simple considerations as indicated in the below. Clearly these general purpose codes are important tools, but sometimes more insight might be gained by small “home-made” codes, hopefully so in the present problem.

The problems stated above can be solved in good approximation by a small Monte Carlo code. The table below provides a list of neutron source energies E_n , of the cross section densities $\Sigma_{\text{tot}}(E_n)$ for neutrons in polyethylene ($\rho=0.95 \text{ g/cm}^3$) and the probability $p(\text{H}(n,p))$ that a first collision results in a proton. Consider non-relativistic kinematics, assume isotropy in the centre of mass system and set $m_{\text{neutron}} = m_{\text{proton}}$. The angular distribution in the laboratory system is then obtained from $\cos \vartheta_L = \cos(0.5 \cdot \arccos(\cos \vartheta_{\text{CM}}))$, where $\cos \vartheta_{\text{CM}}$ is to be sampled uniformly from $[-1,1]$. For stopping powers and ranges of ions in matter see: <http://www.srim.org/SRIM/SRIM2003.htm>, or ICRU 49, data are available from NIST server.

Input data for neutron transport		
E_n	$\Sigma_{tot}(E_n)$	$p(H(n,p))$
keV	μm^{-1}	–
650	$2.364 \cdot 10^{-5}$	0.4623
680	$2.304 \cdot 10^{-5}$	0.4578
710	$2.248 \cdot 10^{-5}$	0.4535
956	$1.872 \cdot 10^{-5}$	0.4255
996	$1.822 \cdot 10^{-5}$	0.4216
1036	$1.753 \cdot 10^{-5}$	0.4153
1256	$1.550 \cdot 10^{-5}$	0.4020
1306	$1.505 \cdot 10^{-5}$	0.3988
1356	$1.464 \cdot 10^{-5}$	0.3959

Alternatively, you could use MCNP© to compute the proton field in the polyethylene converter. Use the PTRAC-card to generate data sets of reaction sites for r_n , the direction of flight of the scattered neutron c_n , and the energy of the scattered neutron E_n , via H(n,n')-reactions. Using non-relativistic kinematics, infer the corresponding direction of flight of the recoil proton c_p and its energy E_p . This yields $f_{conv}(E_p, x_p, y_p, z_p, c_{p,x}, c_{p,y}, c_{p,z})$, (see. Equation (1) and the text following it).

If you wish to tackle this problem but do not have enough time to write the small neutron transport code you can request a small code from the author that produces the proton field in the end plane of the converter and you may also request range tables for protons in the materials used that are based on SRIM2003.

Problem proposed by:

B.R.L. Siebert PTB Braunschweig D, S. Agosteo Politecnico di Milano I

TO PRESERVE THE SCOPE OF THE COMPARISON ON THE EIGHT PROBLEMS, THE PARTICIPANTS ARE ASKED NOT TO PUBLISH THEIR RESULTS IN THE OPEN LITERATURE BEFORE THE FINAL WORKSHOP (AUTUMN 2007).

Correspondence:
Results should be returned to:
Bernd Siebert
 Bernd.Siebert@ptb.de

